Research in Astron. Astrophys. **2010** Vol. **10** No. **9**, 821–866
http://www.raa-journal.org *http://www.iop.org/journals/raa*

Research in Astronomy and Astrophysics

INVITED REVIEWS

Recent results of zebra patterns in solar radio bursts

Gennady P. Chernov

[1] Key Laboratory of Solar Activity, National Astronomical Observatory, Chinese Academy of Science, Beijing 100012, China; *gchernov@izmiran.rssi.ru*
[2] Pushkov Institute of Terrestrial Magnetism, Ionosphere and Radio Wave Propagation, Russian Academy of Sciences (IZMIRAN), Troitsk, Moscow region, 142190, Russia

Received 2010 January 21; accepted 2010 March 26

Abstract This review covers the most recent experimental results and theoretical research on zebra patterns (ZPs) in solar radio bursts. The basic attention is given to events with new peculiar elements of zebra patterns received over the last few years. All new properties are considered in light of both what was known earlier and new theoretical models. Large-scale ZPs consisting of small-scale fiber bursts could be explained by simultaneous inclusion of two mechanisms when whistler waves "highlight" the levels of double plasma resonance (DPR). A unique fine structure was observed in the event on 2006 December 13: spikes in absorption formed dark ZP stripes against the absorptive type III-like bursts. The spikes in absorption can appear in accordance with well known mechanisms of absorptive bursts. The additional injection of fast particles filled the loss-cone (breaking the loss-cone distribution), and the generation of the continuum was quenched at these moments. The maximum absorptive effect occurs at the DPR levels. The parameters of millisecond spikes are determined by small dimensions of the particle beams and local scale heights in the radio source. Thus, the DPR model helps to understand several aspects of unusual elements of ZPs. However, the simultaneous existence of several tens of the DPR levels in the corona is impossible for any realistic profile of the plasma density and magnetic field. Three new theories of ZPs are examined. The formation of eigenmodes of transparency and opacity during the propagation of radio waves through regular coronal inhomogeneities is the most natural and promising mechanism. Two other models (nonlinear periodic space – charge waves and scattering of fast protons on ion-sound harmonics) could happen in large radio bursts.

Key words: Sun: general — Sun: flare — Sun: radio radiation

1 INTRODUCTION

Studies of the fine structure of solar radio bursts are of great importance for both the refinement of the burst generation mechanisms and the diagnostics of the coronal plasma. The most intriguing fine structure is undoubtedly the zebra pattern (ZP) in continuous type-IV radio bursts. The nature of the ZP has been a subject of wide discussion for more than 30 yr. The ZP in the solar radio emission is the simultaneous excitation of waves at many (up to a few tens) of closely spaced, nearly equidistant

frequencies. The basic parameters of ZPs in the meter wave band are represented in the atlas of Slottje (1981). The historical development of observations and theoretical models is assembled in the review of Chernov (2006).

The comparative parameters of ZPs in the different frequency ranges are given in table III in Chernov (2006). Now it is authentically known that in a regular ZP the frequency separation between the stripes grows with frequency: from 4–5 MHz at 200 MHz to $\sim$ 80 MHz at 3000 MHz and to $\sim$150–200 MHz at 5700 MHz. It is important to note that the relative frequency bandwidth of the separate stripe in emission remains almost stably constant with frequency, $\Delta f_{\rm e}/f \approx 0.005$.

Last years' new solar broadband radio spectrometers of NAOC (China, Huairou Station) have allowed us to obtain unique information on a ZP at high frequencies, 2.6–7.6 GHz with high resolution (10 MHz and 5–8 mc) (Fu et al. 2004; Chernov et al. 2001). In the microwave range, the same variety of fine structure was observed. Some events were intensively studied in a series of papers not only for the new features of the ZP but also for their relationship with solar flares and coronal mass ejections (Ning et al. 2000; Huang 2003, 2004; Yan et al. 2007; Huang et al. 2007).

The discovery of the superfine structure of the ZP, in the form of millisecond spikes, was the most significant new effect in the microwave range (Chernov et al. 2003). The probability of such a study strongly grew over the last few years in connection with numerous observations of fast radio bursts (millisecond spikes) during the star flares (Abada-Simon et al. 1995). It is amazing that the period of star spikes in the radio burst of the classical red dwarf AD Leo coincides with the period of spikes in the superfine structure of solar zebra stripes ($\sim$30 ms) (Osten & Bastian 2006).

More than ten different models have been proposed for ZPs; most of them include some emission of electrostatic plasma waves at the upper hybrid frequency $\omega_{\rm uh}$ (Kuijpers 1975a; Zheleznykov & Zlotnik 1975; Mollwo 1983, 1988; Winglee & Dulk 1986; Chernov 2006). The most comprehensively developed ZP models involve mechanisms based on the double plasma resonance (DPR), which assumes that the upper hybrid frequency in the solar corona becomes a multiple of the electron-cyclotron frequency:

$$\omega_{\rm uh} = (\omega_{\rm Pe}^2 + \omega_{\rm Be}^2)^{1/2} = s\omega_{\rm Be}, \tag{1}$$

where $\omega_{\rm Pe}$ is the electron plasma frequency, $\omega_{\rm Be}$ is the electron cyclotron frequency, and s is the integer harmonic number. The model which describes the observations and the conditions in the corona in the best way is the one by Winglee & Dulk (1986), which is based on unsaturated electron-cyclotron maser emission by electrons with a loss-cone distribution.

In order to explain the ZP dynamics in the framework of this mechanism, it is necessary that the magnetic field in the radio source varies sufficiently rapidly, which, however, contradicts the fairly low field values determined from the frequency separation between stripes. Over the last five years, there appeared dozens of papers concerning the refinement of this mechanism, because, in its initial formulation, it failed to describe many features of the ZP. Kuznetsov & Tsap (2007) assumed that the velocity distribution function of hot electrons within the loss cone can be described by a power law with an exponent of 8–10. In this case, a fairly deep modulation can be achieved, but the excitation of waves at multiple DPR levels is still impossible.

In Chernov (1976a, 1990), a unified model was proposed (plasma wave (l) – whistlers (w) interaction: $l + w \rightarrow t$) in which the formation of ZPs in the emission and absorption spectra was attributed to the oblique propagation of whistlers, while the formation of stripes with a stable negative frequency drift (the so-called fiber bursts) was explained by the ducted propagation of waves along a magnetic trap. This model explains occasionally observed transformation of the ZP stripes into fibers and vice versa, but fails to describe the existence of ZP stripes whose frequency is stable over a few tens of seconds.

To overcome difficulties arising in different models, a new ZP theory based on the emission of auroral choruses (magnetospheric bursts) via the escape of the Z mode captured by regular plasma

density inhomogeneities was recently proposed (LaBelle et al. 2003). This theory, however, fails to explain the high intensity of radiation emitted by separate incoherent sources. In addition, the theory imposes some stringent conditions, such as the presence of a large–amplitude ion–acoustic wave.

It is known (Ginzburg & Rukhadze 1975) that the oscillation spectrum of a nonuniform plasma can be discrete; therefore, the existence of a ZP in the solar radio emission can be attributed to the existence of discrete eigenmodes in the nonuniform solar atmosphere. Several aspects of this mechanism were considered in Laptukhov & Chernov (2006); Bárta & Karlický (2006); Ledenev et al. (2006). In Laptukhov & Chernov (2006), dispersion relations were derived for a discrete spectrum of eigenmodes of a spatially periodic medium in the form of nonlinear structures formed due to the onset of thermal instability. The spectrum of eigenfrequencies of a system of spatially periodic cavities is calculated, and it is shown that such a system is capable of generating a few tens of ZP stripes, the number of which is independent of the ratio of the plasma frequency to the gyrofrequency in the source.

In practically all models, the discussion deals with regular ZPs. Problems appear with the interpretation of the frequently observed uncommon stripes of a ZP. For example, for explaining the so-called "tadpoles" (submerged in a developed ZP), special mechanisms were elaborated (Zheleznykov & Zlotnik 1975a; Chernov 2006). Other uncommon forms of ZPs (in the form of zigzags, complex splittings of stripes into their superfine structure) are rarely attempted to explain. They cause big problems for the known models. It is important to note that the model for the whistlers successfully explains the zigzags of stripes and their splittings, and also the variations in the frequency drift of stripes synchronously with the spatial drift of the sources of radio emission (Chernov 2006). Since each new phenomenon issues its uncommon parameters of fine structure, and the entire variety of parameters does not succeed in the associated statistical systematizing, below, primary attention is given to the analysis of separate phenomena. Just such a situation stimulates many authors to elaborate on new mechanisms.

In the present paper, an attempt is made to evaluate which model most adequately describes the new observational data and find out where the ZP stripes form (during the excitation of waves in the source or in the course of their further propagation). Calculations show that the DPR-based mechanism fails to describe the generation of a large number of ZP stripes in any coronal plasma model. Some other unsolved problems or difficulties in the DPR model are also examined in detail in the review.

Here, it is shown that the new varieties of ZPs succeed in explaining these phenomena, within the framework of known mechanisms by taking into account the special features of plasma parameters and fast particles in the source. From another side, the formation of ZP stripes due to the radio wave propagation through the coronal heterogeneities can be recognized as the most natural mechanism of ZPs. The mechanism related to the excitation of discrete eigenmodes of a periodically nonuniform plasma (Laptukhov & Chernov 2006, 2009) can yield the observed number of harmonics. However, in this case, only the possibility of generating harmonics in a one-dimensional stationary problem is considered, i.e., the frequency dynamics of stripes is not analyzed.

During the last three years, some new varieties of ZPs have been recorded. Now it is necessary to estimate the possibility of their interpretation by taking into account all known models of ZPs.

2 NEW OBSERVATIONS

2.1 2004 July 24 Event

Chernov et al. (2008) analyzed strange fiber structures in four events in the decimeter range when small-scale fibers are organized into large-scale ZPs. They used spectral observations from the new Chinese spectrometer (Huairou Station of NAOC, Beijing) in the range of 1.1–2.0 GHz with extremely high resolution of 5 MHz and 1.25 ms (Fu et al. 2004).

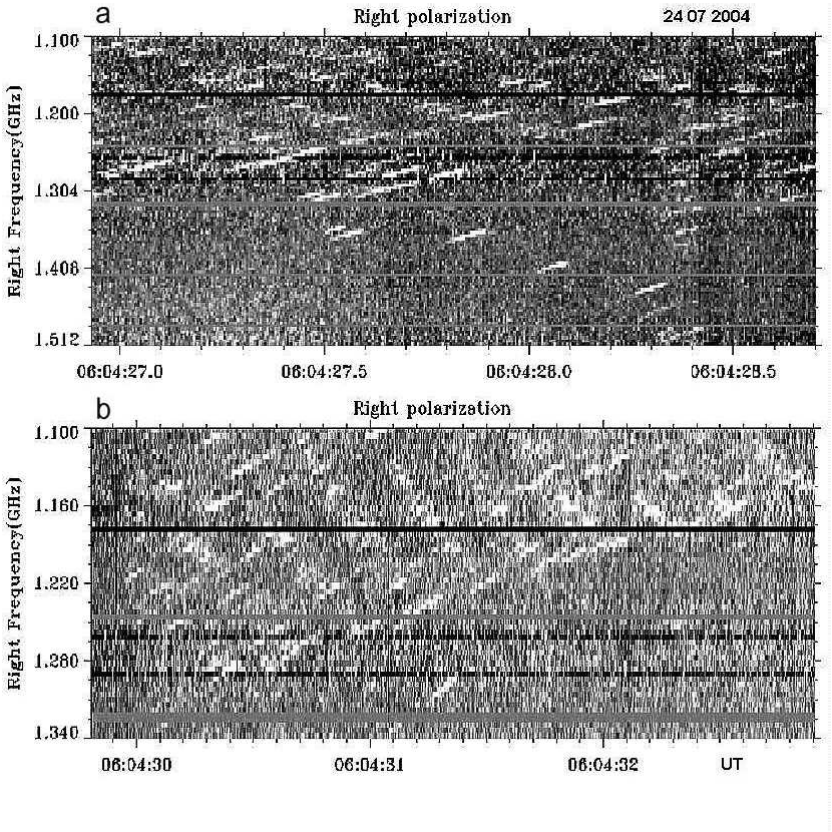

Fig. 1 (a) Dynamic spectrum in the range 1.100–1.512 GHz in left and right circular polarizations recorded by the spectrometer of NAOC on 2004 July 24. (b) The continuation of the 2004 July 24 event in the range 1.100–1.340 GHz in the right circular polarization (the radio emission is fully polarized) (from Chernov et al. 2008).

Figure 1 demonstrates a new variety of stripes in emission in the event on 2004 July 24. At the beginning of the event, separate narrow-band stripes (small fibers) were located along the frequencies, forming almost instantaneous pulsations (around 06:04:20 UT); then they were decomposed and aligned along the inclined straight lines that are parallel to the individual small fibers. At the end of this time interval, the small fibers formed an almost braided ZP (around 06:04:26 UT). The circular polarization of the fibers was dominantly of right-hand sign.

One second later (Fig. 1(a)), they were located once more along the inclined straight lines (06:04:27.0–06:04:28.5 UT), and a new special feature was seen two seconds later (06:04:30 UT): they were localized along the straight lines, but with the reverse (positive) drift. In one more second (06:04:31–06:04:33 UT), this special feature was already clearly the basic prevailing structure (Fig. 1(b)) which is basically regarded as large-scale ZP stripes drifting to higher frequencies with the speed of about 270 MHz s^{-1}. These structures were terminated at a certain high-frequency boundary which drifted to lower frequencies with the speed of approximately –67 MHz s^{-1}.

In Figure 1, only right polarization channels are presented because the polarization degree was 100%. The fiber structure appeared as a forerunner of the rise of continuum which continued for more than three minutes, but no more fine structure was observed.

A flare of M1.0 1F class occurred at 06:01–06:04–06:10 UT in the active region (AR) 10652 (N07W20). The analyzed fiber structure was observed after several strong pulsations at the very beginning of the smooth rise of a flare continuum in the unpolarized emission whose duration was about 5 min.

According to the spectral data of IZMIRAN in the frequency range of 270–25 MHz, the pulsations had a continuation in the meter-wave range in the form of type III bursts, where they stopped at frequencies near 200 MHz in the form of J- bursts. Later, the flare continuum lost any fine structures, and the event ended, without type II bursts or any coronal mass ejections (CMEs).

In the absence of spatially-resolved radio observations, the position of the radio source can be inferred from the image of the flare in the chromosphere of TRACE 1700 Å data (Strong et al. 1994). At the moment 04:07, it was superimposed on the magnetogram (Solar Flare Telescope, NAOJ/Mitaka). Three bright flare kernels were located to the west of the preceding sunspot of this AR, above the quadrupole-like structure of the magnetic field with a peculiar X-point at the center of the flare region.

The two flare kernels were located above the S-magnetic polarity; therefore the radio emission of right circular polarization should correspond to the ordinary wave mode. The flare kernels in the 195 Å images were also located exactly above the bright regions seen in the 1700 Å images, and the radio source in right circular polarization at 17 GHz (Nobeyama Radio Heliograph) was also located in this place. The largest radio flux was recorded in decimeter and meter ranges, indicating the magnetic reconnection occurred high in the corona. As a matter of fact, in the 1700 Å images we see bright tops of the flare loops. The decimeter radio source is expected to be found below the flare current sheet (where the acceleration of fast particles would take place). The positive frequency drift of the large scale ZP stripes may be caused by the downward motion of a plasma ejection from the reconnection region with the Alfvén velocity. On its way, this ejection would meet a flare loop arcade that was expected to be rising. The high-frequency boundary of the termination of emission can be the consequence of this collision.

2.2 2004 November 3 Event

This event was most powerful and most prolonged, with diverse fine structures and duration of about 2 h over the course of repetitive brightenings of the flare. For the analysis, we selected only its first part (with a duration of about 25 min), at the beginning of which small-scale fibers were observed (Fig. 2), and, as in the previous events, it was also a forerunner of the entire event.

The first glance at Figure 2 reveals certain similarity to the event on 2004 July 24: at first, the small-scale fibers occurred chaotically scattered along the frequencies, then they were localized at some frequencies and formed large-scale ZP stripes, and at the end they broke up again to separate into chaotic fibers, which gradually (during $\approx$ 1.5 min) broke up into a cloud of chaotic spikes. The essential difference lies only in different polarizations. Here, it was of moderate right-hand sign.

Figure 3 helps to better estimate the parameters of the small fibers that composed the large-scale ZP. The time profiles at the fixed frequency of 1.216 GHz show that all profiles are symmetrical, and have an almost Gaussian shape. The frequency drift of fibers was stable and constant, $\approx$–270 MHz s^{-1}, and for the large-scale ZP, it was $\approx$630 MHz s^{-1}.

The flare of M1.6 1N class occurred at 03:23–03:35–03:57 UT in AR 10696 (N09E45). The analyzed fiber structure was observed at 03:25:07 UT at the very beginning of the smooth rise of a flare continuum in the non-polarized emission whose duration was about 25 min. According to Culgoora spectral data, strong type II bursts began at 03:33 UT at frequencies near 120 MHz (estimated shock speed 750 km s^{-1}), accompanied by a powerful CME (SOHO/LASCO C2) after 03:54 UT (whose estimated speed was 918 km s^{-1}).

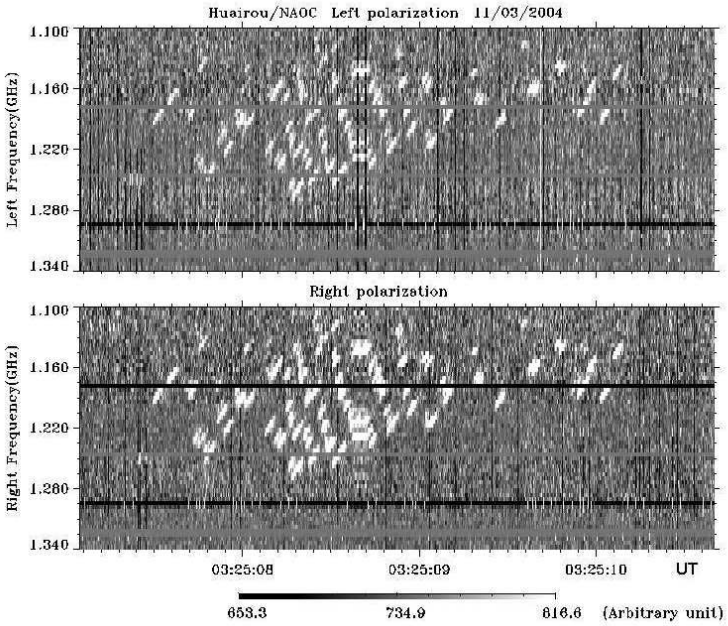

Fig. 2 Beginning of the 2004 November 3 event in the frequency range 1.100–1.340 GHz, showing moderate right-handed polarization: the small-scale fibers are re-grouped into large-scale ZP stripes (from Chernov et al. 2008).

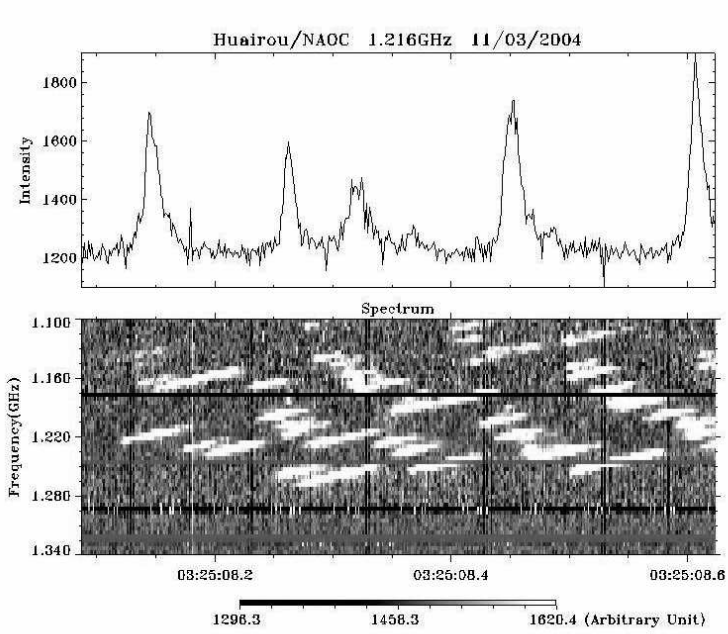

Fig. 3 Magnified dynamic spectrum (*bottom*) and the time profile at 1.216 GHz (*top*) of the fiber structure on 2004 November 3 (from Chernov et al. 2008).

After about 03:30 UT, the polarization of the fine structure changed sign, and the left-handed polarization became predominant. The dynamics of flare processes can be tracked according to RHESSI hard X-ray data in the 6.0–7.0 keV energy band, as shown by the Nobeyama radio map at 17 GHz (Chernov et al. 2008). At 03:26 UT, the radio source had a triple structure (in accordance with the distribution of sunspots in the AR) with a big source of predominantly right-handeed circular polarization above the following spot of the S-polarity. A single HXR-source was located above this radio source. At 03:30 UT, a new HXR source appeared in the south-western portion of the AR. Thus, the strengthening of the radio source at this moment was connected with the development of the flare above the small leading spot of N-polarity. In the higher energy band 14.0–16.0 keV, even two new sources have appeared in the same location. So, it is possible to conclude that the radio emission corresponded to the ordinary wave mode both at the beginning and at the maximum of the event.

We can derive the following conclusions from the observations of two events with small-scale fiber bursts as a substructure of large-scale ZPs:

- Narrowband fibers almost always drift to lower frequencies with the speed that is typical in usual fiber bursts, and sometimes they are similar to the ropes of fibers in the meter range.
- In two events, the fibers evolved from chaotic features in the dynamic spectrum to a regular structure (in the form of large-scale ZP stripes) and again to disorder, being gradually converted into the spike-bursts.
- Large-scale ZPs were limited at high frequencies by a boundary drifting to lower frequencies with the speed of –70 to –90 MHz s^{-1}.
- The radio emission was moderately or strongly polarized and corresponded to the ordinary wave mode.
- The fiber structure appeared as a forerunner of the entire event.
- The fibers, as well as large-scale ZPs, do not reveal absorptions at the low frequency edge.
- A superfine structure in small-scale fibers was not detected with a time resolution of 1.25 ms.

In two other events (2004 December 22 and 2004 October 31) small-scale fibers can be regarded as the fine structure in type III bursts and broadband pulsations (Chernov et al. 2008).

2.3 2006 December 13 Event

2.3.1 Introduction

The most recent large flare of the 23rd cycle was observed on 2006 December 13 (02:10–05:10 UT) in the active region NOAA 10930 (S05W24–27). This was an unusual event by its importance (X3.4/4B) and fast coronal mass ejection (CME). The flare also provided the richest material for the analysis of fine structures of radio emission in the microwave range. Numerous spikes in absorption of millisecond duration are the main feature of radio emission observed during the decay phase of the flare. The Solar Broadband Radiospectrometer (SBRS) in the range of 2.6–3.8 and 5.2–7.6 GHz (Huairou Station, NAOC) carried out the radio observations (Fu et al. 2004). The frequency resolution of the SBRS is 10 MHz, and the cadence is 8.0 ms.

During this long-lasting event, different types of common fine structures were observed (e.g. spikes in emission, usual zebra-patterns and fast pulsations). However, during the decay phase together with the spikes in emission, spikes in absorption began to appear. The latter were first randomly distributed in the frequency range 2.6–3.8 GHz, then they exhibited fast pulsations and trajectories of type III-like bursts in the dynamic spectrum. Furthermore, numerous type III bursts in absorption were observed for about one hour.

The impulsive phase of this event with some fragments of zebra patterns has already been described by Yan et al. (2007). Fast radio pulsations were examined in Tan et al. (2007). They assumed

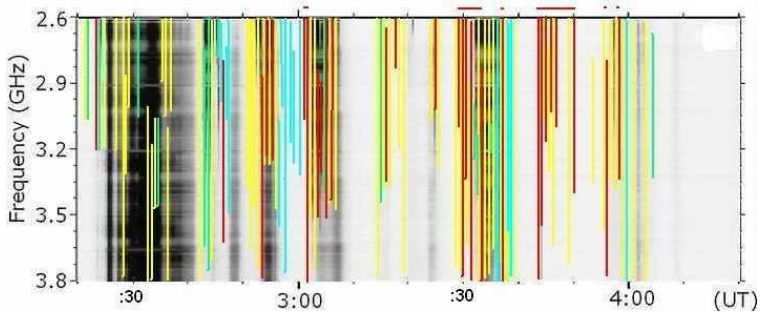

Fig. 4 Dynamic spectrum of the whole event on 2006 December 13 in the frequency range of 2.6–3.8 GHz. The emission is displayed in a negative picture (darker means stronger emission). The color bars indicate timing and frequency range of fine structures: *yellow* – spikes for emission, *red* – spikes for absorption, *blue* – fiber bursts, *green* – zebra pattern. The red horizontal bars at the top show the time intervals when spikes in absorption formed type III-like bursts (from Chernov et al. 2010).

that a resistive tearing-mode oscillation in the current-carrying flare loops modulated the microwave emissions and formed the pulsating structures. The positions of X-points are between two magnetic islands. There are many X-points in each flare loop.

The spikes in emission and fiber bursts were studied by Wang et al. (2008). Chen & Yan (2008) already reported the absorptive spikes in this event. The type III-like burst in absorption had been explained by Chen & Yan (2008) as a fragmentary injection of new particles in a loss-cone leading to quenching of the loss-cone instability of plasma waves at the upper-hybrid frequency. Parameters of the bursts in absorption (instantaneous frequency bandwidth and duration, frequency drift, etc.) depend on parameters of new beams of particles.

A general description of absorptive spikes in this event was carried out by Chernov et al. (2010). The reason for the appearance of spikes in absorption at the decay phase of the event should be understood. It was necessary to estimate how the physical parameters vary in the event, and how the type III-like bursts are formed from the absorptive spikes (with elements of ZP stripes).

The first spikes in absorption appeared at 02:53:08 UT. Further, over more than one hour, different combinations of the spikes in absorption and the type III-like bursts in absorption and in emission were observed. The latter appeared simultaneously and both with positive and negative frequency drift. For the analysis, it is important to know what kind of specific features of the flare were associated with the appearance of bursts in absorption.

Figure 4 shows the timing and frequency range of fine structures in the dynamic spectrum of the whole event. It is evident that spikes in emission (yellow bars) were observed over the whole event while the spikes in absorption (red) were only observed in the decay phase. Typical fragments of bursts in absorption are shown in Figures 6 and 7. It should be noted that the usual fine structures in emission, zebra pattern (green bars in Fig. 4) and fiber bursts (blue bars) were observed over the whole event as well (see also Figs. 8 and 9).

2.3.2 New flare brightening in TRACE images

The further dynamics of the flare was outlined in more detail with the TRACE images in the 195 Å passband. They show flare loops with a temperature of 1.8×10^6 K. Six images taken from the TRACE catalog data (*http://trace.lmsal.com/trace_cat.html*) are shown in Figure 5.

According to the TRACE images of the 195 Å passband at the impulsive phase, the flare consisted of many bright kernels distributed over the entire active region and bright large-scale loops,

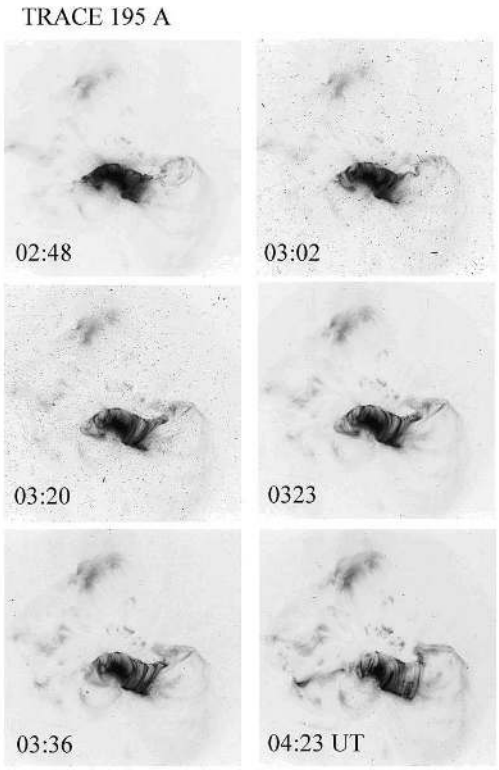

Fig. 5 Development of the flare in the western part of the post-flare arcade in the TRACE EUV passband 195 Å (from Chernov et al. 2010).

which extended predominantly from the north-west to the south-east, connecting to distant spots. During the impulsive phase in the eastern part of the active region, five consecutive flare brightenings were observed. After approximately 02:40 UT, the TRACE images show thin loops (arcades) along the large-scale X-ray loop which began to be formed westwards. After approximately 02:47 UT, the new loops started to appear successively towards the west.

On the first TRACE 195 Å image in Figure 5 (02:48 UT) new bent loops appeared in the western part of the region and began to ascend. The three images (03:02, 03:20, and 03:23 UT) illustrate the subsequent rising of these bent loops and some changes above them which suggest rapid flows. At 03:20 UT the bent loop did look like a cusp for the first time.

After approximately 03:36 UT, the restoration of the magnetic structure began, and the bent loops (with a possible apex) began to descend. At 04:23 UT, the bent loops finally descended, and the burst activity completely ceased after that. During this time, about ten peaks of radio emission occurred at 2.84 MHz (fig. 1 in Yan et al. 2007). Diverse bursts in absorption were observed during practically each peak.

According to the Nobeyama Radio Heliograph (NRH) data at 17 GHz (see fig. 2 in Chen & Yan 2008), the peak of the radio continuum burst was located above the northern flare ribbon in the negative magnetic polarity. During the new flare brightening at 03:28 UT, the radio source revealed asymmetry with a second maximum above the western part of the northern flare ribbon. This location coincides with the new helmet-shaped loop in the western part of the loop arcade after 03:23 UT (Fig. 5).

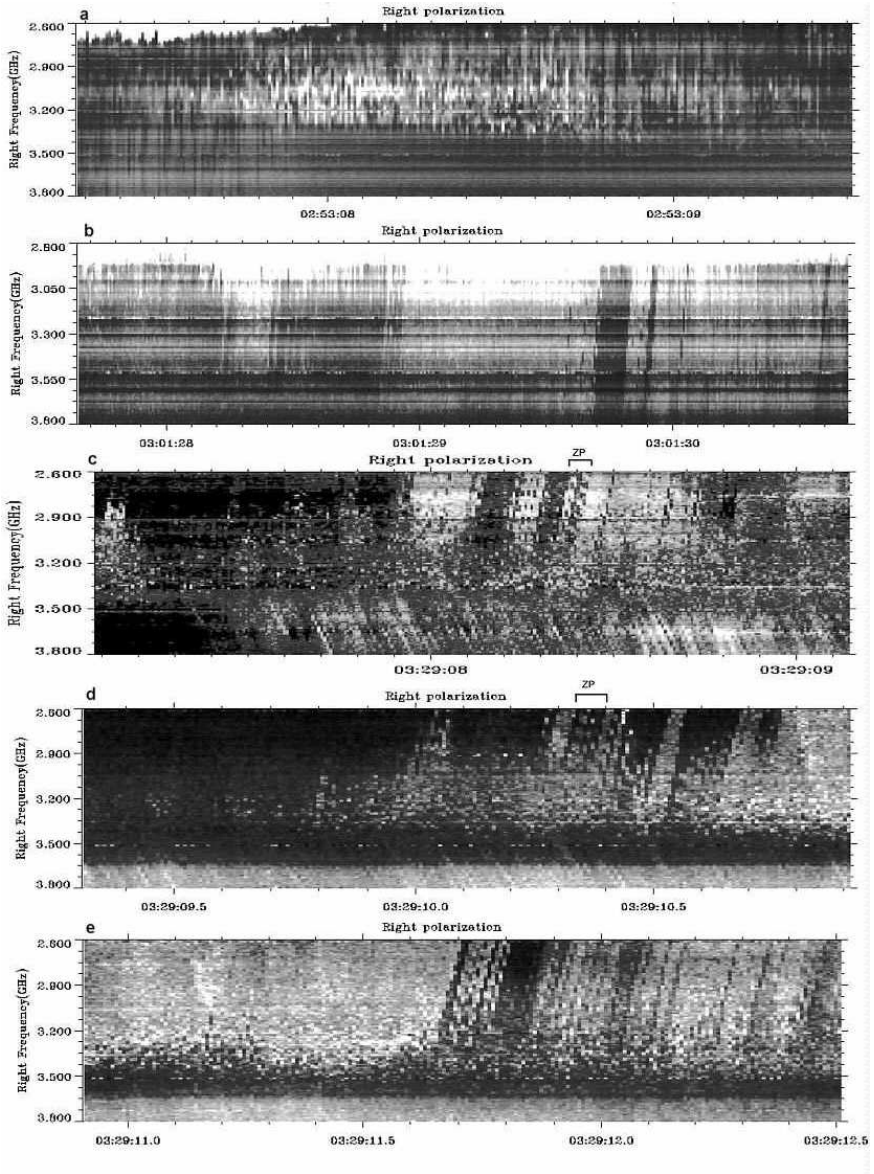

Fig. 6 Dynamic spectra of the component of the right-handed circular polarization in 2.6–3.8 GHz showing the consecutive development of the absorptive spikes at 02:53 UT and of type III-like busts consisting of spikes in absorption at 03:01 and 03:29 UT. The frequency and time scales are different in different panels (from Chernov et al. 2010).

2.3.3 Features of bursts in absorption

Figures 6 and 7 show the appearance and the detailed development in time of spikes in absorption according to the data of SBRS (in the frequency range 2.8–3.6 GHz). Only the right-handed circular polarization (RHCP) components of SBRS are shown because, during the decay phase of the event, the emission was fully right-handed polarized.

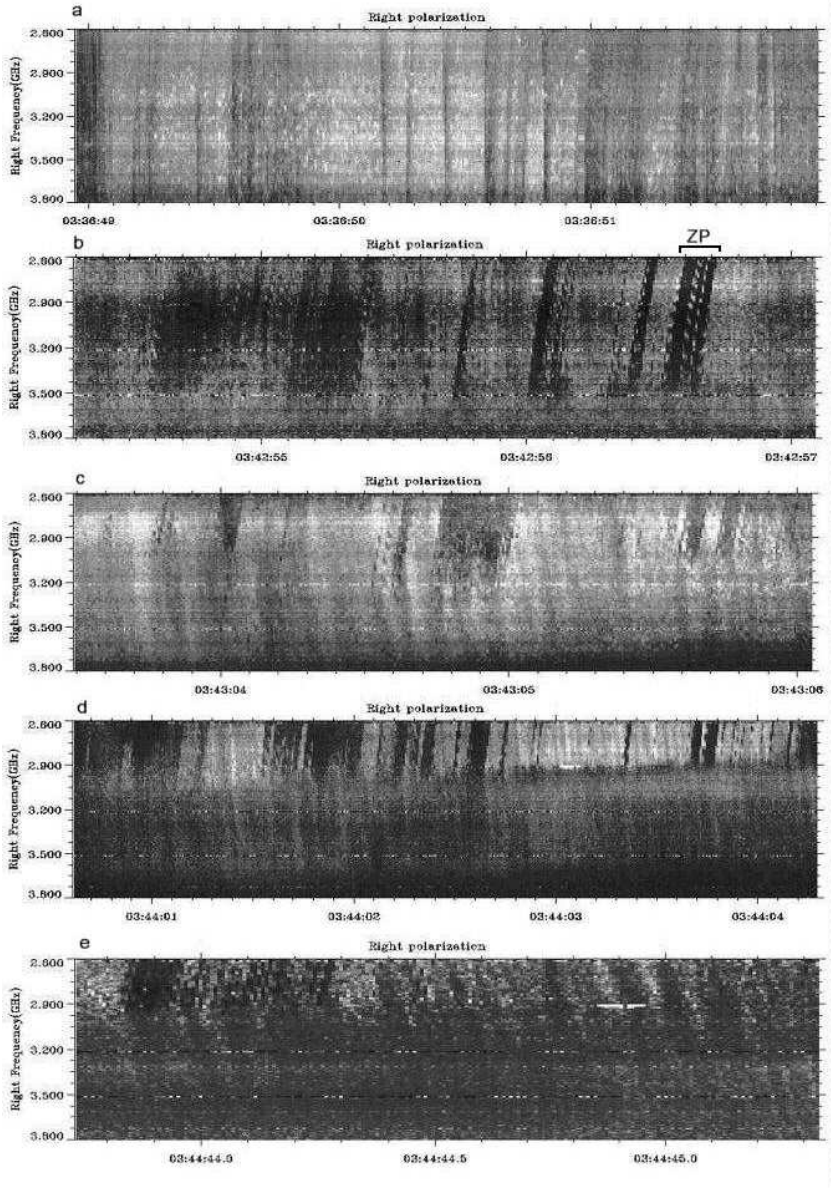

Fig. 7 Continuation of the development of the right-handed circularly polarized component in 2.6–3.8 GHz in the time interval 03:36–03:44 UT showing the absorptive type III-like bursts accompanied by the reverse-drifting bursts in emission and absorption (from Chernov et al. 2010).

The first spikes in absorption appeared at 02:53:08 UT (Fig. 6(a)). All spikes had different frequency bandwidths, from point-like (in one pixel with the size of 10 MHz, 8 ms) to 400 MHz, but no bursts showed frequency drift. Therefore, each spike represents an instantaneous frequency bandwidth. Most of them were scattered randomly in the frequency and time domains. During the time

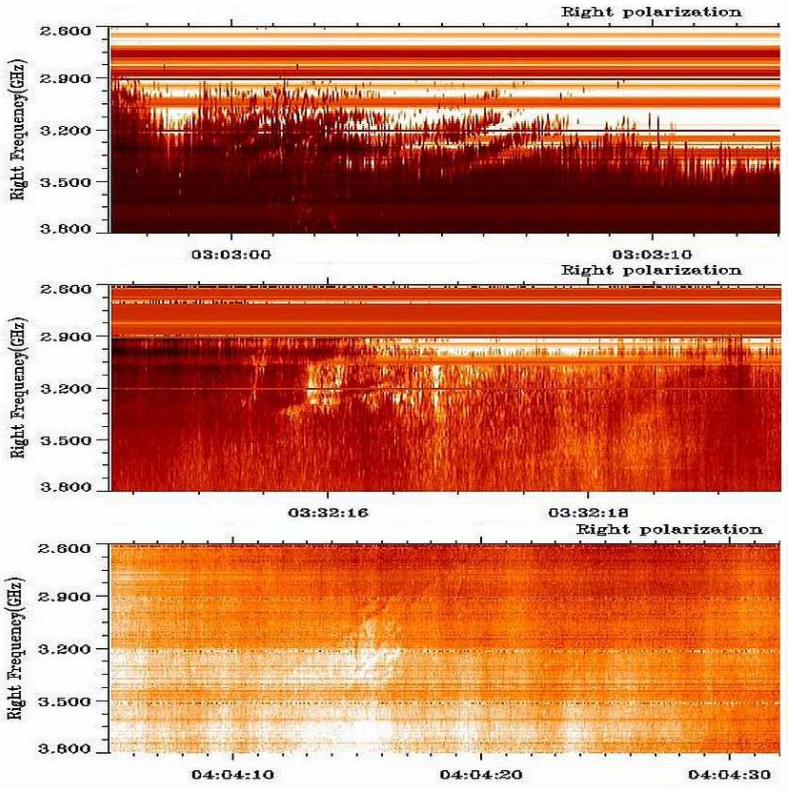

Fig. 8 Enlarged spectra showing the ZP at the post-maximum phase of the event. The top panel shows spikes in emission and absorption superimposed on ZP stripes. The spikes in absorption constituted the absorption stripes of the ZP. Numerous spikes in emission and absorption were accompanied by several ZP stripes in the middle panel. Note the unusual (braided) ZP in emission and absorption in the bottom panel (from Chernov et al. 2010).

interval shown in Figure 6(a), we did not notice specific patterns in the appearance of spikes in absorption or emission. The spikes in absorption and emission appear simultaneously at different frequencies and they are distributed randomly with respect to each other.

After 03:01:28 UT, the non-drifting spikes began to be built along the inclined trajectories and to form the absorptive bursts, similar to type III bursts, shown in Figure 6(b). The analysis of such bursts in the interval 03:01:28–03:01:37 UT is very important. The first group of isolated spikes at 03:01:29.5 UT were built along two type III-like trajectories, with different frequency separations between spikes. Then, the large dark type III-like burst in absorption with a longer duration of 0.12 s appeared. The two subsequent trajectories consisted of isolated spikes again. In addition, several following type III trajectories were accompanied by spikes with diversified frequency bandwidths and frequency drift rates (see the continuation of possibly similar activity in Fig. 6(e)).

It is important to note that the isolated spikes along the type III trajectories were shifted in frequency with separations approximately equal to the bandwidth of the spikes ($\approx$80 MHz). However, in the following type III-like large bursts, they overlapped in frequency (they became more broadbanded, $\approx$160 MHz). The strongest spikes appeared one after another, i.e., with the period equal to their duration (8 ms). Thus, it is not completely excluded that spikes actually have smaller band-

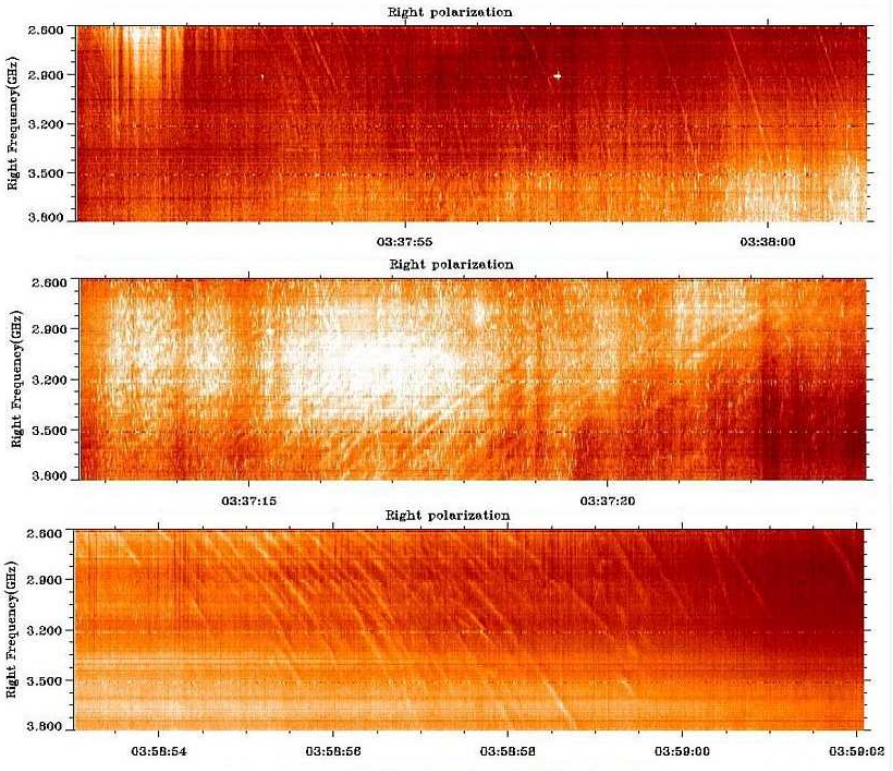

Fig. 9 Fiber bursts at the decay phase of the event. In the three panels, spikes in emission and absorption are superimposed on fibers or are simultaneously visible. The time scales are different in different panels (from Chernov et al. 2010).

widths and shorter duration, due to the limited frequency and time resolution of the instrument (10 MHz and 8 ms). After 03:01:31 UT, clouds of spikes in emission began to appear, with approximately the same parameters, but they did not form type III bursts in emission.

In the interval 03:03:00–03:03:10 UT, fragments of the large-scale ZP in emission appeared in the HF edge of the powerful emission (the top panel in Fig. 8). A large-scale ZP means that the frequency separation between stripes is around 170 MHz, the largest value found in this event (see table 1 in Yan et al. 2007). Numerous spikes in emission and absorption were seen superimposed on ZP stripes. The spikes in absorption constituted the absorption stripes of the ZP. Previously, only spikes in emission were reported as substructures of ZP emission stripes (Chernov et al. 2003; Chernov et al. 2005).

Such a complex combination of different structures continued up to 03:24:30 UT, when the reverse drifting bursts in absorption appeared as the prevailing structure. However, in contrast to type III-like bursts in absorption, they did not show clear spike substructures. To be more precise, maybe the spikes were not resolved by the instrument, or perhaps substructures do not exist at all. Over the next few seconds, the reverse-drifting bursts in emission appeared, and alternated with the bursts in absorption over almost the entire frequency range of the spectrometer. Until 03:25:22 UT, the range of the intermittent reverse-drifting bursts was from 2600 to 3000 MHz.

After 03:29 UT a new powerful flare brightening began, and in the mean time bursts in absorption with new properties appeared (Fig. 6(c)–(d)). The frequency of ≈3400 MHz became the "boundary" between the bursts of the opposite drifts. The bursts in absorption with the fast direct (negative) drift appeared at the higher frequencies, and the reverse-drifting bursts in emission and absorption appeared at the lower frequencies. We did not notice any correlation between bursts with different drifts. Moreover, the drift to higher frequencies of the latter bursts was approximately three times slower, around 3.6 GHz s^{-1}, and they actually looked like classical fiber bursts with typical absorption from their LF edge (Chernov 2006) but with the reverse drift. The low-frequency bursts in absorption were composed of spikes with almost no frequency separation (03:29:08.15–03:29:08.25 UT). The spikes that formed the type III-like bursts had a wide range of parameters and showed no regularity in appearance. The spikes, as the substructures of type III-like bursts, are clearly visible in Figures 10 and 11 with enlarged spectra and time profiles at two fixed frequencies.

However, at 03:29:08.4–03:29:08.5 UT in Figure 6(c) in the type III-like bursts (in the frequency range 2.60–3.05 GHz) it is possible to distinguish absorptive ZP-like stripes (noted on top by symbol ZP), which drifted to higher frequencies and consisted of spikes. A similar but short fragment of ZP-like stripes repeated at 03:29:10.3 in the frequency range of 2.60–2.90 GHz (Fig. 6(d)).

In the subsequent two minutes (03:30–03:32 UT), the powerful pulsations in emission (partially interrupted with broadband pulsations in absorption) and clouds of narrow-band spikes in emission were observed. At 03:32:16 UT, several stripes with a usual ZP appeared (the second panel in Fig. 8) with the narrow frequency separation (of ≈40 MHz). Numerous spikes in emission and absorption accompanied these several ZP stripes.

In Figure 7, further development of bursts in absorption is represented, when the helmet-shaped flare loop on the western edge of the arcade began to descend (the image at 03:36 UT in Fig. 5). In Figure 7(a), pulsations in absorption (or type III-like bursts), are seen against the background of a large cloud of spikes in emission. The pulsations did not reveal a strict periodicity, but the spikes in absorption are visible as the substructures of pulsations.

Against the background of such pulsations during 03:36:57–03:36:58 and 03:37:04–03:37:05.5 UT, the type III-like trajectories containing isolated almost point-like spikes in emission appeared. Again, the classical fiber bursts at 03:37:12–03:37:25 UT against the background of pulsations in emission and absorption were observed (a part of these fibers is shown in the middle panel of Fig. 9), when the flare brightening was decaying. These fiber bursts were gradually transformed into broadband stripes predominantly in absorption with the decreasing frequency drift. Then the reverse-drifting (almost through the entire range) fiber bursts appeared again during 03:37:34–03:37:38 UT. Further, the fibers against the background of powerful pulsations and the clouds of spikes in emission (03:37:49–03:38:10 UT) appeared again.

This entire dynamics is very important for understanding the appearance and development of the uncommon bursts in absorption. During three more minutes, the clouds of strong spikes in emission were observed. At the end of this interval, broadband pulsations in emission and absorption with the reverse drift accompanied these clouds. The pulsations were followed by the type III-like bursts in absorption which consisted of non-drifting spikes in absorption. During the time interval 03:42:56.5–03:42:56.7 UT (Fig. 7(b)), spikes in absorption formed the absorptive ZP-like stripes. In this time interval, all features of the type III-like bursts in absorption noted above (during the different moments) were seen.

The initial HF boundary of the absorptive bursts was slightly displaced downwards, up to ≈3500 MHz. In the middle part of this spectrum, weak non-drifting pulsations with the same HF boundary remained noticeable. The main structure here – the non-drifting spikes in absorption – is the building block of all other forms of bursts (see also Fig. 7(c)). Let us note the basic properties of type III-like bursts in absorption we observed.

– The type III-like trajectories consisted of isolated spikes which overlap, both in frequency (from the HF part) and frequency separation (from the LF part of the spectrum). These single (broken) trajectories appeared prior to the larger dark type III-like bursts, as well as after them.
– In the large absorptive bursts, we were able to count 4–5 sequential trajectories of spikes, which did not show a noticeable frequency-time correlation between them. The drift velocity of type III-like bursts was ≈–12 GHz s^{-1}.
– In several moments, the spikes in absorption in sequential trajectories displaced smoothly to HF, and formed the ZP-like stripes; the maximum duration of stripes was about 0.12 s in the last burst in Figure 7(b). The frequency drift of the stripes was ≈1700 MHz s^{-1}, almost the same as that in the first absorptive ZP-like stripes during 03:29:08–03:29:14 UT.

All these details are more easily visible in enlarged spectra in Figures 10 and 11. Similar short ZP elements drifting like type III bursts (or almost vertical columns) are known in the meter range. For example, Slottje (1972, in his fig. 6(c)) showed numerous almost vertical columns of the ZP. In this case, repeating columns of the ZP can be explained by fast pulsations in absorptions (sudden reductions). Several examples of fast, almost vertical, columns of the ZP in emission (without sudden reductions) were presented in Chernov (1976b) (see also fig. 19 in Chernov 2006). Here, we will examine similar fast elements of the ZP, but in absorption and with a much higher time resolution in the microwave range.

Parameters characterizing the observed spikes in emission and absorption are summarized in Table 1. Let us note that the spikes of type 3 have a more strictly fixed duration of 8 ms and a smaller spread of the frequency bandwidth, and they are repeated strictly through 8 ms.

Table 1 Parameters of Spikes in Emission and Absorption

Type	Range (GHz)[1]	Duration (ms)	Bandwidth BW (MHz)	Relative BW (%)	Period (ms)	Frequency drift
1	0.3–1.2	8–16	10–220	0.3–7.4	8 → 50	|[2]
2	0.3–1.2	8–16	20–400	0.67–13.3	8 → 50	|
3	0.3–1.0	8	30–160	1.0–2.4	8	|
Average absolute error		8	10	0.3	8	

[1] Frequency range inside 2.6–3.8 GHz. [2] - means vertical spikes, the frequency drift approaches infinity. Type 1 – spikes in emission; Type 2 – groups of spikes in absorption; Type 3 – spikes in absorption as substructures of type III-like bursts.

Five seconds after the absorptive type III bursts (at 03:43:03 UT), a new special feature appeared. The HF boundary of bursts in absorption shifted to lower frequencies, down to 3000 MHz (i.e., the radio source must have been displaced upward). Simultaneously, the bursts in emission drifting to HF (or the reverse-drifting type III bursts) with a fixed period ≈ 0.1 s appeared (Fig. 7(c)). Their drift velocity was approximately the same as that in the dark bursts, namely 12 GHz s^{-1}. Then, during almost one minute after 03:43:03 UT, the clouds of spikes in emission began to be superimposed on such structures. From Figure 7(d), it is evident that at 03:44:01 UT a new property appeared: the HF boundary of type III-like absorptive bursts smoothly displaced to lower frequencies; simultaneously the reverse-drifting bursts in emission stopped at the same frequency boundary; in this case they became less prolonged and more frequent (the period became ≈ 0.03 s).

We note that at frequencies higher than the HF boundary, the reverse-drifting bursts continued in absorption and with the period that characterized the reverse-drifting bursts in the emission one minute ago (≈0.1 s). The general appearance of this fragment began to resemble a “herringbone structure” (well known in type II bursts in the meter wave band). The only difference is that it was related to the bursts in absorption. The type III-like burst in absorption and reverse-drifting bursts started at the same frequency, and the starting frequency slowly drifted to the low-frequency region

with a drift rate of about –60 MHz s^{-1}. As indicated by Klassen (1996), this could be a signature of propagating bidirectional electron beams originating near the reconnection area. In our event, the reverse-drifting bursts in emission with their starting frequency below 2.6 GHz may indicate the existence of the second site of acceleration above in the corona. At this time (after 03:36 UT), the cusp-shaped flare loop continued to descend (Fig. 5), and the activity rapidly changed.

After 03:44:05 UT, the bursts in absorption disappeared together with the HF boundary. The reverse-drifting bursts in emission which covered almost the whole frequency range became dominant bursts. During 03:44:41–03:44:44.5 UT the bursts in absorption reappeared, partially with the fragments of the "herringbone structure." This is shown in Figure 7(e), where it is also possible to note that, at the end of this interval, the reverse-drifting bursts (almost over the entire range) in absorption followed. In the course of the subsequent several minutes after 03:44:45 UT, the bursts in emission and absorption in different combinations with the spikes in emission and absorption still existed. In the course of the last flare brightening (03:55–04:05 UT), the bursts in emission (pulsations and spikes) predominated, although the complex forms of bursts in absorption (without type III-like bursts) irregularly appeared.

During 03:58:54–03:58:59.2 UT, the classical fiber bursts with the reverse drift appeared once more (see the bottom panel in Fig. 9). It is remarkable that several stripes of the ZP (with the spiky structure) were observed at the higher frequencies (5.2–5.7 GHz) at this moment. Thus, in the course of the whole period discussed here, the conditions for the excitation of a usual ZP and fiber bursts irregularly appeared. During 04:04:12–04:04:20 UT, the final series of peculiar slow-drifting stripes, exhibiting different absorption and emission characteristics (as elements of the ZP), were observed (the bottom panel in Fig. 8).

After 04:05 UT, several small events appeared in the radio emission at 2.84 GHz (fig. 1 in Yan et al. 2007), but the continuum level gradually decreased to the pre-flare level.

2.3.4 Time profiles of bursts in absorption

Figure 10 shows the enlarged spectrum of the sharpest type III-like bursts in absorption at 03:42:56 UT whose duration was $\approx$ 0.7 s. The intensity profiles at two frequencies (2.85 and 3.06 GHz) clearly show the modulations due to the bursts in emission and absorption. In terms of the absolute scale in solar flux units (s.f.u.), the maximum flux in emission reached 330 s.f.u. and the minimum flux (in absorption) $\approx$ 240 s.f.u. with the average level of the continuum of $\approx$ 280 s.f.u. The maximum of modulation depth at frequency 3.060 GHz was observed between the spike in absorption at $\sim$ 03:42:56.60 UT and the spike in emission 03:42:56.68 (about 80 s.f.u.).

Between the three type III-like bursts in absorption, the ZP looks like the classical one (Chernov 2006): the increased emission in the bright stripes (two high peaks on the profiles) and the moderate absorption in the dark ones (here the absorption is even with respect to the average level of flux in the type III-like bursts in absorption). In the spectrum of Figure 12, another property of the usual ZP is clearly seen: the smooth increase with frequency of the frequency separation between the stripes. It increased from $\approx$80 MHz at the frequency of 2700 MHz to $\approx$150 MHz at 3400 MHz.

In the type III-like bursts consisting of isolated spikes in absorption (for example, a trajectory at 03:42:56.3 UT), the instantaneous frequency bandwidth of the spikes also increased with frequency from of 30 to 100 MHz. The decreasing frequency separation between them disappeared at the frequency of $\approx$3400 MHz. The latter was not coordinated with the frequency separation of the absorptive stripes of the ZP. However, at other onsets noted above for similar bursts, this property was not observed.

The ZP-like stripes appear to be parallel. We can distinguish six stripes against the background of type III-like bursts in absorption (they are marked by thin black lines in the spectrum) and three stripes from the LF edge remained diffuse. However, this conclusion depends on many factors: on

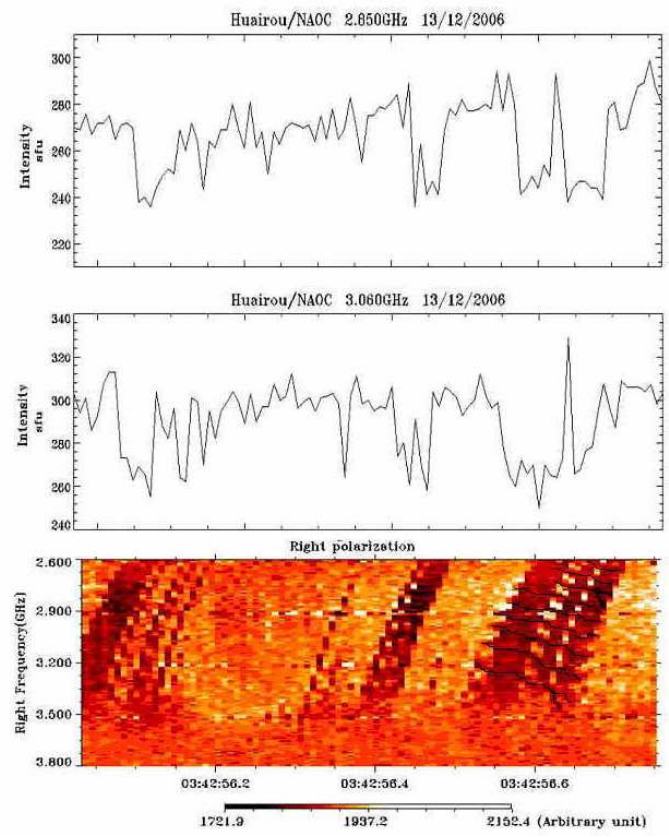

Fig. 10 Enlarged spectrum and time profiles at two fixed frequencies (2.85 and 3.06 GHz) of ≈ 0.7 s duration showing the modulations during the type III-like bursts in absorption with a ZP. The absorptive ZP-like stripes are marked by thin black lines (from Chernov et al. 2010).

the conditions in the radio source and on the rate of particle acceleration in different parts of the radio source. The precise measurements of the frequency drift showed that its speed also increased with the frequency: from 1000 MHz s^{-1} to 1700 MHz s^{-1}. Thus, it is possible to say that this was a usual ZP, but it was observed against the background of type III-like bursts in absorption. The ZP-like absorptive stripes remained noticeable even against the background of the type III-like absorptive bursts.

Figure 11 shows the distribution of the spikes in absorption in the background of another type III-like burst in absorption. The spikes were distributed randomly, but they tended to form several short stripes. Such structures in the spikes were called 'braided ZP' by Slottje (1981) (see the event 1970–07–27) and 'lace bursts' by Karlický et al. (2001) because of the variety of the ZP.

2.3.5 Brief conclusion from observations

In spite of the complexity of the analyzed phenomenon, let us isolate the basic properties of the bursts in absorption.

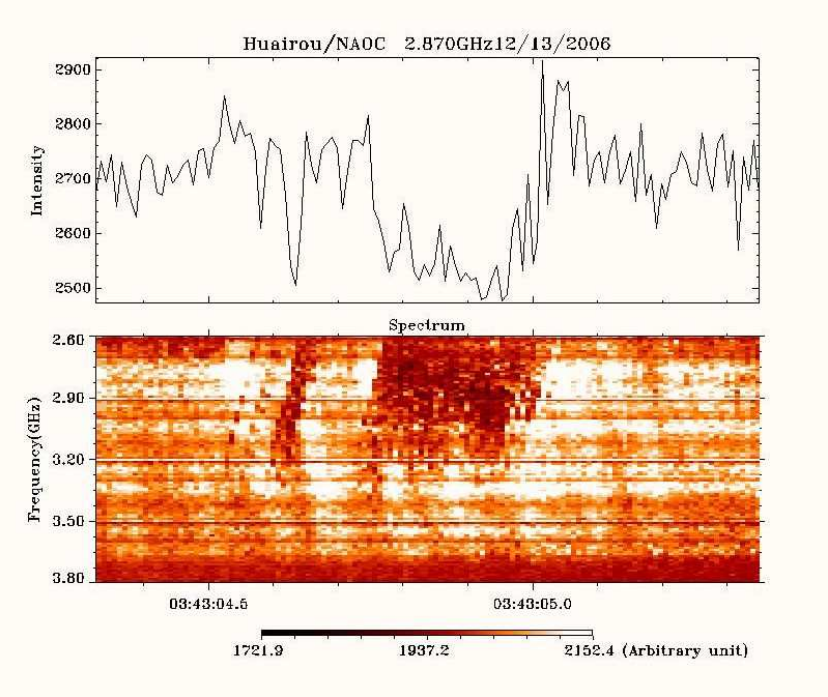

Fig. 11 Enlarged spectrum and time profile of ~ 1 s duration at a fixed frequency of 2.87 GHz, showing the modulations during the type III-like bursts in absorption. The intensity scale is in arbitrary units. The spikes, as the substructures of type III-like bursts, are clearly visible (from Chernov et al. 2010).

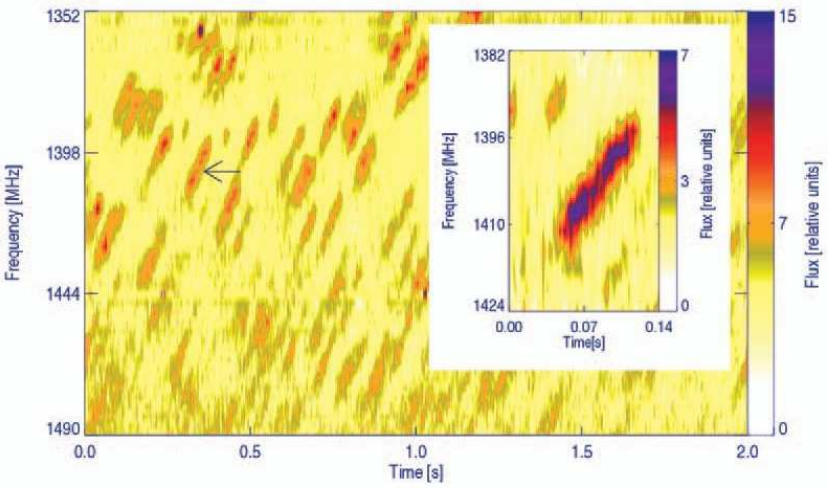

Fig. 12 Dynamic radio spectrogram of the dm radio spikes recorded on 2001 October 30, beginning at 12:20:27 UT (from Dąbrowski et al. 2005).

- The basic structural element (a building block) of all bursts in absorption was the spikes whose duration was close to the limit of the instrument's resolution (8 ms) and the instantaneous frequency bandwidth was on average ≈70–80 MHz.
- The dynamics of appearance and development of spikes is very rapid. It changed every several seconds.
- The type III-like bursts in absorption were basic structures of the absorptive spikes. In three brief moments, the absorptive spikes created ZP-like stripes which lasted for 0.1 s.
- The complex combinations of the drifting bursts in emission and absorption sometimes exhibited the form of a 'herringbone structure.'
- The activity of absorptive bursts alternated (or were simultaneously observed) with the usual fine structure in emission: spikes, broadband pulsations, ZPs and fiber bursts.
- This entire interval of the peculiar fine structure was observed during several flare brightenings in the western part of the flare arcade above the south magnetic polarity. We believe that during this time the magnetic reconnection probably took place. The right sign of polarization corresponded to the ordinary wave mode.
- The bursts in absorption were sometimes observed in the meter-wave range (Chernov et al. 1998), but the event discussed here for the first time revealed a wide variety of absorptive bursts in the microwave range.

2.4 Other Events

Small fibers similar to ones shown in Figure 1 were observed by Dąbrowski et al. (2005) (Fig. 12). However, the authors discuss them as drifting spikes. Dynamical radiospectrograms of the spikes were recorded in the 1352–1490 MHz frequency band which was split into 46 channels, each 3 MHz wide. The time resolution of the collected data is equal to 80 μs, the highest ever obtained. The observations of the radio spikes have been collected with the 15 m radio telescope at the Torun Centre for Astronomy, Nicolaus Copernicus University in Torun, Poland. The observed radio spikes have internal structure and form chains (rope-like fibers and braided ZPs). They occurred during the bulk motion of the plasma along the long loops, observed with the TRACE telescope in the 171 Å band.

Another kind of spike (called dot emissions) was observed with the Brazilian Solar Spectroscope (Mészárosová et al. 2008) in the dm range of 950–2640 MHz with variable time and frequency resolution between 10-1000 ms and 1–10 MHz, respectively. An example of a group of dot emissions arranged as zebra-like chains observed on 1999 March 19 is shown in Figure 13 (as a part of fig. 1 from Mészárosová et al. 2008). Figure 13(b) presents a global view of the dot emissions. The time and frequency resolution is 100 ms and 5 MHz, respectively. Figure 13(c) reveals a detailed view showing the dot emissions with undulating chains resembling the zebra pattern. Figure 13(d) shows the radio flux in time at 1400 MHz where peaks with an intensity of $\sim$ 130 SFU correspond to individual dot emissions (horizontal line in Fig. 13(c)).

Figure 14 shows an example of the structural evolution of the group of dot emissions observed on 1999 October 19. This group starts with some irregular dot emissions (panel a), but later they evolve into almost regular fiber-like (panel b) and zebra-like (panel c) chains. At the end, the group of dot emissions again becomes irregular (panel d). During times of dot emission, no background burst emission was detected.

Sych et al. (2006) and Zlobec & Karlický (2007) studied the characteristics of the zebra-associated spike-like bursts during the 2003 August 5 event that were recorded by the Ondrejov radio spectrograph in the range 1–2 GHz with time resolution of 100 ms (upper panel in Fig. 15). Simultaneously, the spiky structure was examined using the 1420 MHz polarization profiles of the Trieste Astronomical Observatory with a very high time resolution of 1 ms (bottom panel in Fig. 15).

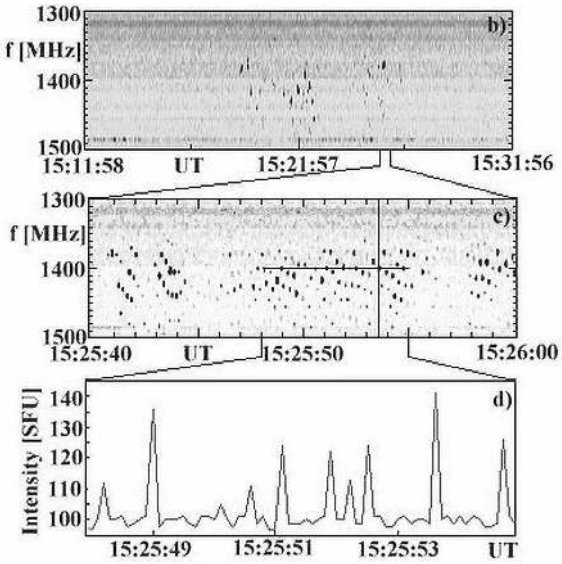

Fig. 13 Dot-emissions (*in black*) arranged as zebra-like chains observed on 1999 March 19: b) global view of dot emissions, c) zebra-like chains, d) radio flux in time at 1400 MHz (*horizontal line* in c) (from Mészárosová et al. 2008).

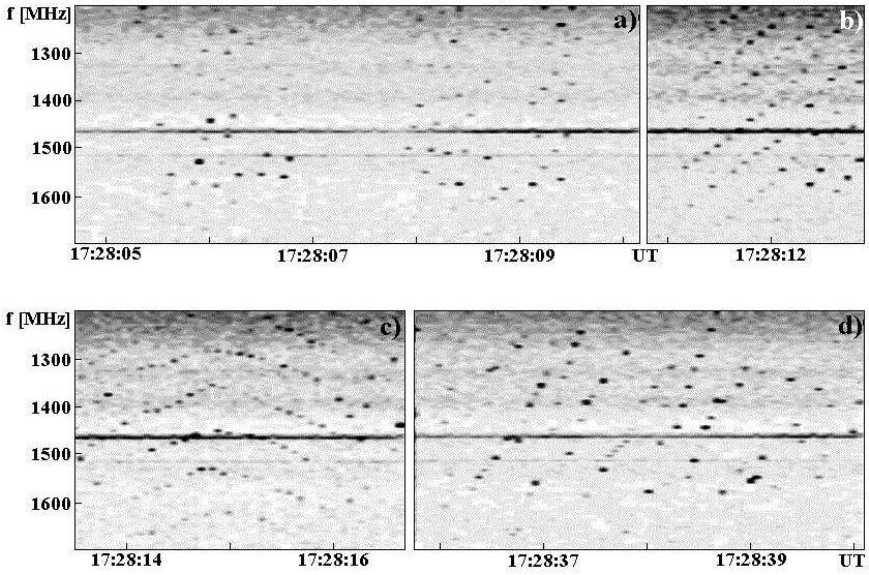

Fig. 14 Example of the arrangement of the series of dot emissions (*in black*) observed on 1999 October 19: irregular dot emissions (a), fiber-like chains (b); zebra-like chains (c), and irregular dot emissions (d) (from Mészárosová et al. 2008).

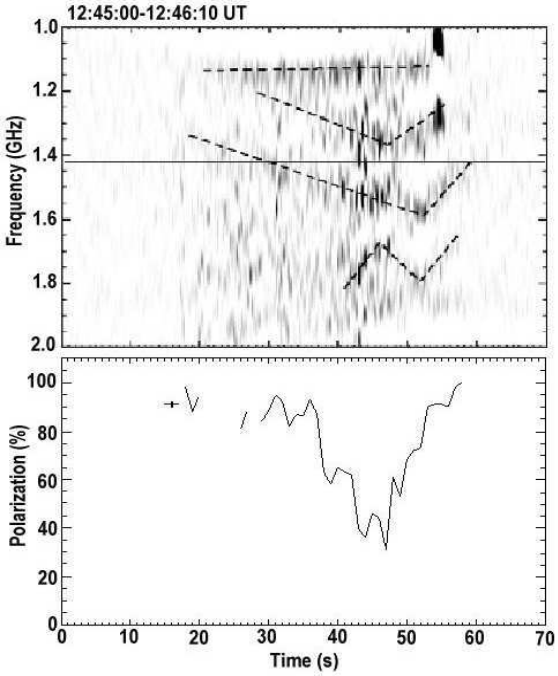

Fig. 15 *Upper panel*: Part of figure 5 from the paper by Sych et al. (2006) showing the time evolution of the spike-like bursts clustered into zebras forming a "V" like structure (in the event from 2003 August 5). *Bottom panel*: contemporaneous time evolution of the mean polarization (in an R-sense) of the selected spike-like bursts at 1420 MHz (from Zlobec & Karlický 2007).

The selected spike-like bursts show a duration (with a mean value of about 7.4 ms at half power) and it is not influenced by the polarization. For the selected bursts, there was just a "tendency" that the weaker component (L- polarization channel) should be delayed. Zlobec & Karlický (2007) realized that the L continuum was generally low with respect to the R continuum; however, the polarization of the spikes does not always match the contemporaneous polarization of the continuum.

The observed superfine structure (spikes) of zebras can be interpreted as proposed by Chernov et al. (2003). Nevertheless, Zlobec & Karlický (2007) think that the model based on the double plasma resonance (DPR) as proposed by Bárta & Karlický (2001) and Karlický et al. (2001) is also possible. Namely, this model explains both the zebras and the spikes by the same double plasma resonance process; the spikes are generated by the interruption of the DPR process by assumed turbulence (density or magnetic field variations).

Magdalenić et al. (2006) reported supershort structures (SSSs), in particular as substructures of the ZP and as tadpoles in the range 265–350 MHz using the solar radiospectrograph Artemis IV (Greece) with a time resolution of 10 ms (Fig. 16). The spikes in the ZP exhibit a duration of 11 – 13 ms, shorter than what was reported earlier in the meter range. Tadpoles are comprised of an emission "eye" with a duration of $\approx$50 ms at the high-frequency side of the burst and a stretched absorption "body" with a bandwidth of $\approx$40 MHz. In spite of distinctive differences (the emission tails of the tadpoles are not visible), the Slottje (1972) tadpoles and these tadpole-like SSSs belong to a class of physically equivalent bursts.

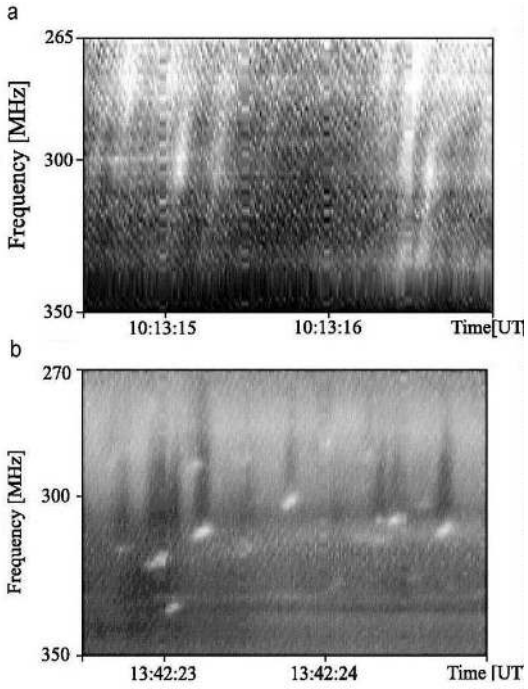

Fig. 16 Artemis IV dynamic spectra of negatively drifting supershort structures (SSSs) in the background of the ZP with a superfine structure (a) and tadpole-like bursts (b) in the event on 2000 April 15 (from Magdalenić et al. 2006).

3 GENERAL DISCUSSION OF THE EVENTS

3.1 2004 July 24 and November 3 Events

Small-scale fibers differ from usual fiber bursts only by narrow total frequency bandwidth and they are similar to ropes of fibers, therefore the usual (that is, most accepted) mechanism for fiber bursts should work, namely the coalescence of a plasma wave (l) with whistlers (w): $l + w \rightarrow t$ (Kuijpers 1975b; Chernov 1976a, 1990). However, the propagation of whistlers is limited by a small magnetic trap in the form of fast shock fronts escaping from a region where magnetic reconnection occurs (Chernov 1997). In our case, the periodicity of fibers was not so evident, and fibers were organized as large-scale stripes of a ZP. So, these ZP stripes become visible only when whistlers propagate through the ZP source.

In our events, the radio sources cannot be point-like ones, since in such a case one whistler wave packet should produce all zebra stripes simultaneously, but we did not see such a feature. Since the small fibers were not connected by a unique straight line in the dynamic spectra, we cannot assume that one whistler wave packet passes through several DPR levels consecutively in an extensive source. So, the unique possibility remains that whistlers are excited at the same DPR level simultaneously with the plasma waves. Without whistlers, ZP stripes cannot be visible, at least in the DPR model with a loss-cone distribution function, in accordance with numerical results of electrostatic instability in Kuznetsov & Tsap (2007). Whistlers without a plasma wave cannot be detected either, but a plasma wave of low energy will be sufficient (at places of DPR) to emit radio waves of sufficient intensity. Thus, whistlers "highlight" DPR levels.

In order to confirm this hypothesis, let us estimate the magnetic field strength B in two ways. One is from the observations of separate fibers using the model of the whistlers, and the other is from a large-scale ZP in the DPR model. If the hypothesis is correct, these values of the field strengths should be equal.

From the whistler model for small fibers, we have $\Delta f_{\rm e} \approx f_{\rm w} \approx 0.1\ f_{\rm Be}$ ($f_{\rm w}$ is the whistler frequency), and a mean value $\Delta f_{\rm e} = 12.5$ MHz (for the events of July 24 and November 3), and we obtain $B \approx 45$ G.

In the DPR model, the frequency separation depends on the scale heights of density ($N_{\rm e}$) and magnetic field ($L_{Ne} = 2N_{\rm e}\ (dN_{\rm e}/dr)^{-1}$ and $L_B = B\ (dB/dr)^{-1}$) (Zlotnik et al. 2003):

$$\Delta f_s / f_B \approx L_B / |L_{N{\rm e}} - L_B|. \tag{2}$$

For Δf_s =72 MHz (for the November 3 event) we could obtain about the same value B = 46 G for $L_{N{\rm e}} = 1.4 \times 10^9$ cm and $L_B = 5 \times 10^8$ cm. In the flare region, the plasma is very inhomogeneous and such scale heights are realistic. In our events, only 3–4 large-scale stripes of a ZP (or DPR- levels) are simultaneously formed in the spectrum which demonstrates the small sizes of local $L_{N{\rm e}}$ and L_B in flare inhomogeneities. Four DPR levels are simply produced at harmonic numbers $s = 10 - 14$ with such a ratio of scale heights.

The stable frequency drift of fibers implies that the magnetic field changes little during the lifetime of the structure (Chernov 1990). The frequency drift of fibers is mainly determined by the group velocity ($\upsilon_{\rm gr}$) of whistlers, and we have $\upsilon_{\rm gr} = 2c \times f_{\rm Be}/f_{\rm Pe} \times [x(1-x)^3]^{1/2}$, where $x = f_{\rm w}/f_{\rm Be}$ is the ratio of whistler frequency to cyclotron frequency (Kuijpers 1975a). If we assume the parameter x varies little during the lifetime of the structure, and $f_{\rm Be}/f_{\rm Pe}$ has a consistent value due to the DPR condition, then $\upsilon_{\rm gr}$ would vary little and consequently the whistlers would cause a stable frequency drift of fibers, at least within a certain DPR level. Therefore, the positive frequency drift of a large-scale ZP can be connected with the downward motion of the source. In the absence of a good analytical model of electron concentration in the upper chromosphere, we will use a graphical representation given, for example, in the model of Allen (in fig. IV.1 of Krüger 1979). Utilizing the dependence of plasma frequency ($f_{\rm Pe}$) on height (r), it is possible to roughly estimate the value of the gradient of $f_{\rm Pe}$ between 1000 and 2500 MHz to be on the order of 240 MHz/10^8 cm. Then, we can use the simplest expression for the definition of the velocity of propagation:

$$V \approx 2 \frac{df/dt}{f} \frac{N_{\rm e}}{dN_{\rm e}/dr} = \frac{df/dt}{df_{\rm Pe}/dr}. \tag{3}$$

The frequency drift df/dt = 630 MHz s^{-1} will correspond to the velocity of about 2590 km s^{-1}. Such a value might be more than a typical Alfvén velocity. Therefore, it is possible to assume that the plasma ejection that moves downward from the magnetic reconnection region has caused a shock wave.

In the July 24 event, the drift of 220 MHz s^{-1} implies the velocity $\approx$ 900 km s^{-1}, which is somewhat more than the Alfvén velocity ($V_{\rm A} \approx 700$ km s^{-1}for the estimated value of $B = 45$ G).

The drifting boundary of the emission termination at the high frequency edge of a large-scale ZP may mean that a moving shock front meets a rising closed magnetic loop. So, the conditions for DPR are satisfied only in a narrow height interval, below the magnetic reconnection region, and only at the very beginning of events. After such a collision, they will be destroyed, and large-scale zebra stripes will be transformed into a braided ZP (Fig. 1(b)). Thus, the radio source showing such a fiber structure differs from the radio source of the rope of fibers only by the absence of a magnetic trap (only one shock front) where fast particles could make periodic bouncing motions, and by short lived conditions for the DPR. The absence of any absorption is simply explained by the absence of continuum emission at the very beginning of events. Only the pulsations in the October 31 event

were observed against a weak continuum, and we could detect some fragments of absorption between fibers (fig. 6 in Chernov et al. 2008).

Thus, we assume that the usual mechanisms can be applied for the interpretation of such a fiber structure: the coalescence of whistler waves with plasma waves producing fiber bursts and the DPR-model for large-scale ZPs. However, the following special features of the plasma wave excitation in the radio source must be present. Both whistler and plasma wave instabilities are too weak at the very beginning of the events (the continuum is almost absent), and the fine structure is almost invisible. Moreover, according to the recent simulations of Kuznetsov & Tsap (2007), the fast electrons with a loss-cone distribution cannot excite a high enough level of electrostatic waves in the DPR levels, so that the separate stripes would be visible. Then, whistlers generated directly at the DPR levels by the same fast electrons will "highlight" the radio emission only from these levels due to the interaction with plasma waves and we observe small-scale fibers as a substructure of a ZP. More precisely, the whistler packets may bring about sufficient plasma wave energy as well as a new composition of the particle distribution, therefore the DPR levels could be more pronounced and "highlighted."

Wu et al. (2007) interpreted the small-scale fibers in the November 3 event as drifting spikes emitted from "solitary kinetic Alfvén waves" (SKAWs) by fast electrons accelerated by the electric field and trapped in SKAWs. However, they did not discuss the reasons for the formation of fibers along the stripes of large-scale ZPs. Furthermore, the source of the strong Alfvén waves, which accelerates a large fraction (≈ 0.1) of the background electrons at the beginning of the event, also was not examined.

We have not adopted the model of LaBelle et al. (2003), since it is supposed to be applied to the explanation of a large number of stripes with a narrow frequency separation. In the large-scale ZP in question, on the contrary, the frequency separation is considerably wider than in the usual ZP. Recent evaluation by Chen & Yan (2008) on the validity of the mechanism of LaBelle et al. (2003) indicated that, with the realistic values of the density contrast (with $\delta \leqslant 0.2$), the model cannot account for the large number of ZP stripes.

However, we cannot completely exclude the possibilities of application of the new models, based on the existence of the bands of transparency and opacity when the radio waves propagate through a spatially periodic medium (for example, Laptuhov & Chernov 2006). It is possible that the large-scale ZP is the result of this selectivity with the specific scale of thermal heterogeneities, which move downward from the flare region, and small-scale fibers are caused by additional quasi-periodic modulation of these heterogeneities, for example, by a fast magneto-sonic wave propagating from below. Or alternatively and more simply, the radio waves meet on their way to the small- and large-scale heterogeneities which move in different directions, i.e., a radio wave is filtered by transparency bands twice. These possibilities require more detailed study.

3.1.1 Other events

Considering all aspects of the observed dot emissions, Mészárosová et al. (2008) think that the dot emissions are generated in a similar way as zebras (Ledenev et al. 2001) or lace bursts (Karlický et al. 2001). Thus, they propose that the dot emissions are produced in the solar atmosphere at the locations where the so-called double plasma resonance condition (1) is fulfilled. The upper-hybrid waves at these locations can be generated, e.g., by the anisotropic beam ($T_\perp > T_{||}$, where $T_\perp$ and $T_{||}$ are the temperatures of energetic electrons across and along the magnetic field, respectively) accelerated during the flare's primary energy processes. The beam anisotropy can be naturally formed along magnetic field lines by an escape of fast electrons from slower ones. Then these upper-hybrid waves are transformed to electromagnetic waves (with the frequency $\omega_{\rm el} \approx \omega_{\rm uh}$ or $\omega_{\rm el} \approx 2\omega_{\rm uh}$), which are observed by radiospectrographs on the Earth. This process is a resonant one which means that its intensity can be several orders of magnitude higher than those associated with non-resonant

processes. This can explain the fact that, at times of dot emission, no background burst emission was detected.

Using this model, we can explain not only individual dot emissions, but also their chains. The beam along its trajectory generates dot emissions in several resonance locations (s-harmonics). The higher s means a higher height of the dot emission source in the solar atmosphere. Thus fiber-like chains of dot emissions can be formed. On the other hand, zebra-like chains of dot emissions can be explained by a sequence of anisotropic beams producing dot emissions nearly at the same position on the same s-harmonic. Even the whistler waves, which are considered in the model of fibers, can enhance emission at the locations with double resonance conditions. Therefore, both forms of zebra-like and fiber-like chains are possible.

Due to similarities in morphology and characteristic properties between the dot emissions and dots in the fine structures of zebras and fibers, Mészárosová et al. (2008) think that both have a similar physical origin. They found that fiber-like chains of the dot emissions evolve into zebra-like chains and vice versa. These changes are in agreement with the idea of Chernov et al. (1998) who proposed that both the zebras and fibers are generated by whistler packets. The propagating whistler packets may also generate dot emissions at the positions in the solar atmosphere where the double resonant conditions are fulfilled (see also, Sawant et al. 2002; Krishan et al. 2003). Furthermore, they propose that the chaotic character of some groups of dot emissions is due to rapidly varying plasma parameters (in the MHD turbulence) in the region of dot-emission sources.

3.1.2 2006 December 13 event

From the observations discussed above in detail, we are able to understand the reason for the appearance of the spikes in absorption, as well as the variable nature of their parameters. The main task is to explain formation of the absorptive type III-like bursts and absorptive ZP-like stripes of the absorptive spikes, in combination with different bursts in emission.

Let us recall that the loss-cone instability is the most probable mechanism of the continuous radio emission of the type IV bursts (including microwave bursts). Plasma waves are excited at the upper hybrid frequency by the fast electrons, captured in a magnetic trap, where the particle-velocity distribution with the loss-cone is formed (Stepanov 1974; Kuijpers 1975a; Zhelezhyakov 1995; Kuznetsov & Tsap 2007). The maximum amplification of waves occurs under the conditions of double plasma resonance (DPR, when the upper hybrid frequency is close to integer harmonics of the electron cyclotron frequency). The appearance of a usual ZP and fiber bursts during the entire event attests to the fact that the loss-cone velocity distribution actually existed.

The dips in emission (corresponding to bursts in absorption) mean the quenching of the loss-cone instability. According to Zaitsev & Stepanov (1975), Benz & Kuijpers (1976), and Fleishman et al. (1994), this quenching can occur because of additional injection of fast particles, which fill the loss-cone. The process of the quenching of instability is examined in detail in a recent paper by Chen & Yan (2008). The authors showed (Fig. 17) that the beam with a linear dimensions of $\approx$ 220 km and a Maxwellian particle-velocity distribution inside the loss-cone causes absorption with a frequency bandwidth of $\approx$60 MHz (due to the cyclotron self-absorption of upper-hybrid waves). The calculated absorptive depth corresponds to the observed value: the modulation in the growth rate in Figure 17 corresponds exactly to the observed absorption depth of $\approx$17% in our Figure 10. Let us note that according to the calculations by Kuznetsov & Tsap (2007), the beams with the power-law spectrum with a large spectral index should give bursts in emission (the spiky superfine structure of the ZP stripes).

Taking into account the fact that absorptive spikes do not always follow type III trajectories, and that they are often a random collection of instantaneous bursts, it is natural to assume a random acceleration of small-scale beams occurs. The dimensions of the beam would then determine the

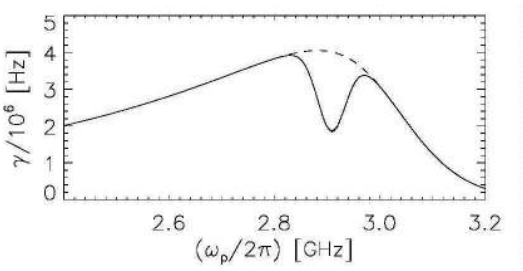

Fig. 17 Dependence of the total growth rate γ of the upper hybrid waves on the plasma frequency. The initial growth rate result corresponds to a value of $s = 15$. Signs of an absorption feature with a frequency bandwidth of about 60 MHz can be clearly seen (from Chen & Yan 2008).

instantaneous frequency band. The quenching of instability occurs only when the instability develops in the location of the beam. Then the beam rapidly leaves the region, and the emission will be restored there. Most likely, the maximum effect is achieved in the DPR conditions. Therefore, when the moving beam reaches a neighboring DPR level, a certain space between the spikes in absorption will be formed. By this method, it is possible to explain the discrete nature of absorptive spikes. Various parameters of the absorptive spikes can be associated with different local gradients of density and magnetic field. At the beginning of the interval of bursts in absorption, the spikes in absorption were still accompanied by spikes in emission with similar parameters (Fig. 6(a)). It means that at this moment not all beams were confined in the trap. This untrapped part of the beams would have given off bursts of emission, although the beams did not move ahead further, possibly, they were reflected.

In the mildly inhomogeneous corona, the DPR levels are the surfaces whose size perpendicular to the line of sight is more than 10 000 km. Compared to this size, the magnetic loops are very narrow and inhomogeneous in density, so that the DPR levels in the adjacent loops cannot coincide with each other. If the beams of particles were periodically injected along one loop, then we should always see ZPs. Therefore, most likely they are injected consecutively in time and simultaneously in several loops. In cases like this, we would often observe almost random distributions of spikes in the type III-like bursts (Fig. 11). However, if the DPR levels almost coincide among the adjacent loops, then a smooth displacement of dark spikes would be produced, and at these moments the ZP will appear. The frequency drift of the ZP stripes ($\approx$1700 MHz s^{-1}) can be explained by an appropriate displacement of the DPR levels in the corona. Even a slow downward motion of a loop making a sharp angle with respect to the gradient of plasma frequency (which exactly occurred, according to the TRACE images in Fig. 5) could lead to rapid lowering of DPR levels in the corona, which will also explain the frequency drift of ZP stripes. During the resistive tearing-mode instability (see below), the condition of frozen magnetic flux is disrupted, and magnetic field lines can move independently of the plasma (Aschwanden 2004).

The beam traveling between the DPR levels can give impulsive contributions to the emission of the Cerenkov resonance, so that the appearance of bright ZP stripes (spikes in emission) is entirely expected (the plasma mechanism of type III bursts). The frequency drift of type III-like absorptive bursts ($\approx$ 12 GHz s^{-1}) would correspond to the speed of the electron beam not exceeding 10^{10} cm s^{-1} in accordance with Allen's density model of the corona (see fig. IV.1 in Krüger 1979).

Wang et al. (2008) considered that the spikes in emission are generated by the electron cyclotron maser (ECM) mechanism. However, the majority of spikes with right circular polarization were observed during flare brightening in the northern flare ribbon in the south magnetic polarity. Thus, the radiation mode was ordinary. Two episodes with left circular polarization were connected with

the brightening in the southern flare ribbon (see the black rectangle in fig. 3(b) of Wang et al. 2008) where the north magnetic polarity could be dominant. This also means the ordinary wave mode dominates, while in the ECM radiation the extraordinary mode should dominate (Fleishman & Melnikov 1998). For this very reason, the estimations of the magnetic field strength obtained by Wang et al. (2008) in the ECM model almost exceed by an order of magnitude the ones obtained by Yan et al. (2007) using the frequency separation of ZP stripes.

The simultaneous presence of bursts in emission and absorption with different drift rates (Fig. 7(c)–(d)) testifies that at least two places of particle acceleration exist at the different heights. In accordance with Figure 5 (the pictures at 03:23 and 03:36 UT), we can assume that above the cusp-loop, in the course of the post-flare restoration of the magnetic structure, a magnetic island was probably formed, and particle acceleration occurred in the two current layers located above the flare cusp-loop (upward) and above the magnetic island (downward). Such an assumed scheme coincides with the sketch of the magnetic configuration proposed for this flare in figure 8 in Guo et al. (2008).

As Schwenn et al. (2006) diligently noted, despite many decades of indirect observations suggesting the presence of a current sheet, such as soft X-ray cusp structures (Tsuneta 1996) and horizontal inflow, direct observations of the formation and evolution of a current sheet in the solar atmosphere have been missing. Strong observational evidence for reconnection comes from the post-eruption emission and dynamics. Our radio observations also testify to the probable case for reconnection in the erupting solar corona.

The rise of helmet-shaped loops in three TRACE images at 03:02, 03:20 and 03:23 UT in Figure 5 allows us to propose the existence of a single X-point above the helmet-shaped loop, and the initiation of flows due to the magnetic reconnection. The consecutive flows may be associated with the formation of magnetic islands above the helmet loop. The sketch of the magnetic configuration can be similar to figure 8 of Pick et al. (2005) as a two-dimensional cut of the three-dimensional configuration across the twisted flux rope. Similar two-dimensional magnetic configurations were often discussed in many numerical simulations (Tsuneta 1996; Lin & Forbes 2000; Aschwanden 2004 and references therein). The three-dimensional flux rope is in fact anchored (line-tied) to the photosphere. The theory of three-dimensional reconnection is presented in greater detail in the book of Priest & Forbes (2000). The two-dimensional representation is mostly done for convenience, but the magnetic structure is three-dimensional (see fig. 4 in Roussev et al. 2003 for a view of the very complicated magnetic field configuration). All special features of two-dimensional reconnection, enumerated in Pick et al. (2005), are also valid in our case. In the framework of an erupting flux rope, magnetic reconnection occurs behind the twisted rope. The accelerated particles form beams along the newly reconnected field lines and propagate both upward and downward.

Two places of acceleration, separated in height, suggest the tearing-mode instability, in that two (or more) magnetic islands were formed and the entire activity at the post-eruptive phase is associated with the restoration of the magnetic structure.

The analysis of microwave pulsations by Tan et al. (2007) confirms such an evolution of the flare. They concluded that the flaring region consisted of many current-carrying compact loops. In each current-carrying flare loop, the resistive tearing-mode instability will trigger the formation of a series of multi-scale magnetic islands. The X-point is located between the two magnetic islands. The opposite frequency drifts of pulsations also suggest the particle acceleration occurs in the opposite directions.

The radio bursts drifting in the opposite directions in the frequency coverage of the spectrograph (Fig. 7(c)–(d)) indicate the simultaneous existence of two places of particle acceleration in the current sheets between the magnetic islands. The fast particles moving from the higher to the lower corona are responsible for the type III burst in emission with the reverse drift. The fast particles moving from the lower to the higher corona are seized in the magnetic trap and give off the type III-like bursts in absorption with negative drift.

Karlický & Bárta (2007) found that electrons are accelerated most efficiently in the region near the X-point of the magnetic reconnection at the end of the tearing process and the beginning of the restoration of the magnetic configuration.

In this connection, all intervals of new peaks in the burst profile at the decay phase (fig. 1 in Yan et al. 2007) were very rich in spikes of absorption, type III–like bursts consisting of spikes in absorption and usual ZPs and fiber bursts with different frequency drifts (see Figs. 6–9). The appearance of ZPs and fiber bursts means the loss-cone velocity distribution of fast particles inside the radio source (magnetic islands) exists.

The beams, accelerated above the flare loop would have propagated upward and fallen into the magnetic trap, where the loss-cone distribution of fast particles was already present, and would have caused bursts in absorption. The particles accelerated above the magnetic island would have probably propagated along the overlying magnetic loops downward (where the loss-cone distribution was absent). They might have simultaneously produced the reverse-drifting bursts in emission. The comparison of spectra in Figure 7(b)–(d) suggests a slow lift of the lower site of particle acceleration, which may have created a kind of 'herringbone structure.' After $\approx$ 03:44:01 UT, the reverse-drifting bursts in emission were stopped by the drifting boundary (a hump of the 'herringbone structure'). At higher frequencies, their continuation transformed to bursts in absorption (though their relationship is not very clear). The loss-cone distribution was probably formed there up to this moment and the quenching of instability by additional beams already became the main effect.

The difference in the parameters of these bursts in absorption (they were prolonged, broad-banded and diffuse) indicates that these beams were larger in scale and their velocity dispersion was wide ($\approx$1). The velocity dispersion in the beams, critical for the spikes in absorption, was much less than 1. New beams with great longitudinal velocities stimulate the whistler generation at the anomalous Doppler resonance and, as a consequence, the formation of ZP stripes in emission (in Fig. 10 at 03:42:56 UT) could be explained in the whistler model (Chernov 1996).

When the slowly drifting boundary became almost indistinguishable at 03:44:44 UT, the diffuse reverse-drifting bursts in absorption covered the whole frequency range (2.6–3.8 GHz), and the spikes in absorption almost disappeared. At this moment, the existence of the magnetic island must have ended.

4 NEW THEORIES OF ZPS

4.1 What is New in Improved DPR-based ZP Theories?

The mechanism proposed in LaBelle et al. (2003) can be regarded as an important step in attempts to improve the DPR-based model. The escape of the Z mode is considered at one DPR level (a point radio source), whereas the harmonics are assumed to be eigenmodes that propagate through regular inhomogeneities, such as an ion-acoustic wave. The number of harmonics is large only if density variations in the ion-acoustic wave reach $\sim$20%. However, as was shown in Chen & Yan (2008), it is hardly possible that such a strong ion-acoustic wave can be generated in the solar corona; in fact, the amplitude of density variations is no more than $\sim$2%. In this case, only several ZP stripes can be generated by this mechanism, whereas up to a few tens of stripes are usually observed. In our opinion, a disadvantage of this theory is that it fails to explain the high intensity of radiation emitted by separate incoherent sources.

In the basic papers on the DPR theory (Zheleznyakov & Zlotnik 1975; Winglee & Dulk 1986) the velocity distribution function of fast particles was assumed to be narrow, with an infinitely small spread in velocities; therefore, calculations of the growth rates of upper hybrid waves could hardly provide a realistic picture (Chernov 2006). Besides, Winglee & Dulk (1986) restricted themselves by consideration of the Maxwellian distribution of particles over momentum that could significantly affect the results obtained. This was clearly demonstrated in Kuznetsov & Tsap (2007), where the

following electron distribution function of the loss-cone type was chosen (see Fig. 18):

$$f_p\,(p,\,\theta)\,=\,\varphi\,(p)\,\begin{cases} 0,\ \theta\leqslant\ \theta_c\,-\,\Delta\theta_c \\ \frac{\theta\,-\,\theta_c\,+\,\Delta\theta_c}{\Delta\theta_c}\,, \qquad \theta_c\,-\,\Delta\theta_c\,<\,\theta\,<\,\theta_c, \\ 1,\ \theta\,>\,\theta_c \end{cases} \tag{4}$$

where the function $\varphi(p)$ describes the electron distribution over momentum and θ_c is the loss-cone boundary with a width $\Delta\theta_c \ll 1$.

In old papers, the term associated with the velocity spread, to be more exact, the spread over particle momenta ($\Delta p/p$), was left in the expression for the anti-Hermitian part of the plasma permittivity. In the course of the new analysis, Kuznetsov & Tsap (2007) conclude that the non-relativistic approximation cannot be used for investigation of the generation of upper-hybrid waves at the double plasma resonance when $s \gg 1$. The authors used the condition of the cyclotron resonance of waves and accelerated electrons in the form:

$$\dot{\psi}_s = \omega - \frac{s\omega_B}{\Gamma} - k_z v_z = 0\,, \tag{5}$$

where $\dot{\psi}_s$ is the time derivative of the phase difference between the waves and the gyrorotating particles, v_z is the longitudinal component of electron velocity (v), and $\Gamma = (1\,-v^2/c^2)^{-1/2}$ is the relativistic factor.

Here, it is necessary to recall that Zlotnik et al. (2003) assume that the dispersion relation (A.6) is correct only inside the hybrid band. They obtained a very narrow maximum of the growth rate due to the estimation of $\Delta k_\perp/k_\perp$; the velocity dispersion $\Delta v_\perp/v_\perp$ was missed as the infinitesimal quantity. This was already examined in detail in Chernov (2006). Zlotnik et al. (2003) assume also that many authors (Winglee & Dulk 1986; Kuznetsov & Tsap 2007) erroneously conclude that the kinetic instability of plasma waves described by the dispersion relation (A.6): $\omega^2 \cong \omega_p^2 + \omega_B^2 + 3k_\perp^2 v_T^2$ may contain several harmonics, while it is valid only inside the interval $\Delta\omega \leqslant \omega_B$. This assertion is correct, mainly, without taking into account relativistic correction and for the strictly perpendicular propagation. Zlotnik & Sher (2009) showed that in this case the harmonics, which adjoin the hybrid band on the top, give the overstated contribution to the value of increment, and this leads to the expansion of its maximum. To answer this question, new calculations with the precise dispersion relation will only help. At least, Kuznetsov & Tsap (2007) assert that comparison with the exact solution of the dispersion relation shows that the equation of upper-hybrid waves (A.6) describes the behavior of the oscillation branch with normal dispersion well, even at $\lambda \geqslant 1$, including the frequencies above the hybrid band. Moreover, Robinson (1988) has shown that weakly relativistic effects (especially in the case of *slightly non-transversal propagation*) cause the branches with normal dispersion corresponding to different harmonics to reconnect to one another at $\omega \approx s\omega_B$. As a result, a single continuous branch is formed. In addition, the condition of touching of the loss-cone boundary and the resonance curve can be satisfied only for one certain value of s. Since the contribution of the term associated with this harmonic will considerably exceed the contribution of other terms in the sum for the loss cone with a sharp boundary (when $\theta_c \to 0$; see the following), we can neglect the summation over harmonics and assume that the growth rate $\gamma \approx \gamma_s$, where γ_s is the growth rate at the s-th harmonic.

In the course of the analysis, Kuznetsov & Tsap (2007) derived the final form of the imaginary part of the dielectric permeability (in the relation for γ):

$$\begin{array}{l} \mathrm{Im}\,\varepsilon_{||}^{(s)}\ \approx\ -2\pi^2 m^4 c^2\,\frac{\omega_p^2}{k^2}\,\frac{n_b}{n_0}\,\Gamma^3 J_s^2\,\left(\frac{k_\perp p_\perp}{m\omega_B}\right)\,\times \\ \left[\frac{\partial\varphi(p)}{\partial p}\ +\ \frac{\varphi(p)\,\tan\theta_c}{p\Delta\theta_c}\,\left(\frac{s\omega_B}{\Gamma\omega\,\sin^2\theta_c}\ -\ 1\right)\right]\,\frac{\Delta p_z}{p}\,, \end{array} \tag{6}$$

where the momentum $\boldsymbol{p} = (p_z; p_\perp)$ and the parameter Γ correspond to the point of tangency $p_{\perp 0} = p_{z0}\,\tan\theta_c$ (see Fig. 18); $J_s(\xi)$ is the first-order Bessel function.

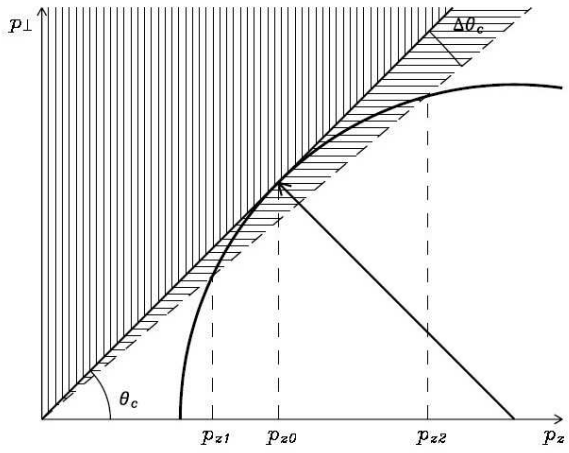

Fig. 18 Schematic of the loss-cone distribution and the resonance curve in the space of electron momenta (from Kuznetsov & Tsap 2007).

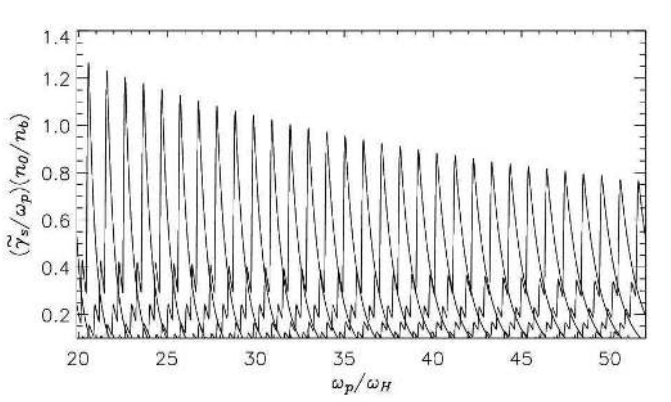

Fig. 19 Dependence of the maximal growth rate of upper-hybrid waves on the plasma parameters for the power-law distribution of electrons over momentum (from Kuznetsov & Tsap 2007).

The derivation of Formula (6) somewhat differs from the corresponding procedure in the work of Zheleznyakov & Zlotnik (1975) because of another normalization condition for the function $f\boldsymbol{p}(\boldsymbol{p})$ and a misprint in the tensor of the dielectric permeability by the coefficient in front of the matrix (which contains the relativistic electron mass ($\tilde{m}$) rather than the rest one (see appendix in Kuznetsov & Tsap 2007).

As a result of calculations, for the Maxwellian distribution of particles over momentum ($\phi_1(p) = A_1 \exp(-p^2/2p_h^2)$) of the loss-cone type (4) and real values of the velocity spread ($\sim$0.1), the modulation depth between the peaks of the growth rates turns out to be too small. However, calculations performed with a power-law velocity distribution function with an index of power of 8–10 yielded a modulation depth that was quite sufficient for the ZP formation at many harmonics (Fig. 19).

A steep power-law spectrum of particles can be considered as an analog of a small velocity dispersion, although such spectra are sometime observed, especially in repeated bursts of hard X-ray emission (data from RHESSI).

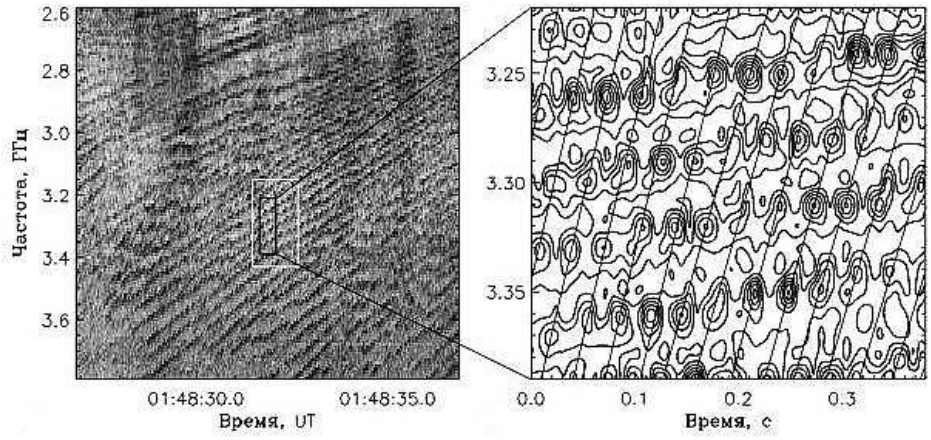

Fig. 20 ZP in the frequency range 2.6–3.8 GHz in the event 2002 April 21. The magnified fragment of the spectrum (on the right) demonstrates the superfine structure of stripes in the form of periodic millisecond spikes, which, for better visualization, are shown by contour levels of the intensity (from Kuznetsov 2007).

Kuznetsov & Tsap (2007) and Kuznetsov (2007) applied their results to interpret 34 ZP stripes with a superfine structure in the form of millisecond spikes in the 2.6–3.8 GHz frequency range (Fig. 20) under the assumption that the electron beams were generated strictly periodically. It is important to note that the straight lines, which connect spikes in the adjacent ZP stripes (in the right panel in Fig. 20) can be drawn at any inclination. Thus, the velocity of beams can be any value, and it is selected arbitrarily.

However, if we consider the possibility of simultaneous excitation of waves at 34 DPR levels in the corona, assuming that the plasma density depends on the altitude by the conventional barometric formula $f_{\rm P} = f_{\rm P0} \exp[-(h - h_{\rm B0})/10^4 T]$ and the magnetic field by the formula derived in Dulk & McLean (1978) from the radio data, $B = 0.5\ (h/R_{\rm s})^{-1.5}$ where $R_{\rm s}$ is the Sun's radius, then we obtain that 34 DPR levels extend in the corona up to altitudes of ∼65 000 km, which, according to current knowledge, correspond to the plasma frequency ∼250 MHz.

We calculated the DPR levels shown in Figure 21 by using a barometric formula with the commonly accepted coronal plasma parameters: the electron temperature $T_{\rm e}$ = 1.2 × 10^6 K and the initial plasma frequency $f_{\rm P0} = 3800$ MHz at the altitude $h_{\rm B0}$ = 20000 km. If we use a dipole dependence of the magnetic field for cyclotron harmonics, then the DPR resonances at harmonics with $s \geqslant 50$ will occur at altitudes higher than 100 000 km. Thus, the simultaneous excitation of waves at 34 levels in the corona is impossible for any realistic profile of the plasma density and magnetic field (if we do not assume it to be smaller, so that it is on the order of magnitude of the local density and magnetic field scale heights). For example, if we assume that the magnetic field decreases with altitude more slowly (see, e.g. fig. 55 in Zheleznyakov 1995), then there will only be a few DPR levels at low harmonics. It should be noted that, as a rule, only the first several cyclotron harmonics are easy to excite, whereas the excitation of harmonics with $s > 50$ is hardly possible.

In this connection, let us note that in the following paper (Kuznetsov 2008) the author proposed an alternative mechanism: a model in which the superfine temporal structure is formed due to modulation of the radiation by downward propagating MHD oscillations. The wavelet analysis showed a decrease of the period of spikes (from 40 ms at 2.6 GHz to 25 ms at 3.8 GHz). Variation of the observed period of oscillations is caused by a variation of the speed of the DPR levels (due to the Doppler effect). It was found that in the considered event on 2002 April 22, the MHD oscillations should have a period of about 160 ms and a speed of about 1500 km s^{-1}. This model allows us to explain the observed variation of the pulse period with the emission frequency.

At the same time, the frequency drift rate of the zebra stripes (increasing with an increase of the frequency from 60 to 160 MHz s^{-1}) was explained by the upward moving DPR levels. The observed polarization degree was connected with a partial depolarization when the emission propagates through a region with a transverse magnetic field. Both of these last effects were often used in many other papers (other events). However, there cannot be a universal interpretation because the frequency drift is often oscillating (like a saw-tooth) and the degree of polarization may be very different (sometimes with a change of sign during the event).

However, the superfine stripe structure in the form of millisecond spikes is apparently produced during the generation of the primary continuum radio emission, rather than arising in the course of ZP formation. This is confirmed by the detailed analysis of the time evolution of the spectral amplitudes of continuous radiation several seconds before the appearance of the ZP. It is seen from Figure 22 that, when there is not yet regular ZP stripes, the time dependence of the radiation intensity at the frequency 3.19 GHz clearly exhibits regular spikes with a period of ∼30 ms. This period is then present in the ZP (see Fig. 20). Thus, the superfine structure is not a consequence of wave excitation at DPR levels.

The superfine structure was also observed in the meter wavelength range. It was shown in Chernov et al. (1998) that such a spiky structure can arise due to periodic acceleration of fast particles provided that the simultaneous splitting of the ZP stripes is caused by the excitation of whistlers under the conditions of normal and anomalous Doppler effects (new beams).

Zlotnik et al. (2009) give an analysis of the occurrence of zebra patterns in fast drifting envelopes of continuum absorption, based on radio spectra of the Astrophysical Institute Potsdam, shown in Figure 23. For the explanation of a ZP in fast drifting (type III burst-like) envelopes, it is proposed that we should consider complementary multinonequlibrium components of the coronal plasma in the DPR model. ZPs should be related to the emergence of fast particle beams. However, prior to the electron beam emergence, the nonequilibrium plasma consists of two components: one having a loss-cone distribution f_1 with velocity υ_1 and causing the background continuum and another one f_2 of DGH type (Dory et al. 1965) with velocity υ_2 being able to provide the DPR effect and thus causing the ZP.

The loss-cone component is denser and cooler than the DGH component. Thus, for many reasons, the stronger continuum can dominate the zebra pattern, making it invisible in the dynamic spectrum. If the electron beam emerges, it fills the loss cone, quenches the loss-cone instability (according to Zaitsev & Stepanov 1975), and causes a type III-like burst in absorption. The switch-off of the continuum during the electron beam passage makes the zebra pattern visible against the absorption burst background. Some specific parameter conditions should be fulfilled:

- for the zebra structure excitation by the DGH component f_2 (υ_2/υ_T ∼15–30), there exist reasonable intervals of velocity $\upsilon_1 \sim$ (1/6–1/2)υ_2 and electron number density $N_2 < N_1 <$(10^2–10^7)N_2 for the component f_1 where the proposed generation scheme is valid;
- $N_\mathrm{b} \gg N_1$ is a necessary condition for the absorption burst;
- the proposed scenario is only valid if the beam velocity ($\upsilon_\mathrm{b} \approx c/3$) is much greater than the bulk velocity of electrons in the loss cone ($\upsilon_2/\upsilon_1 \approx$3–6) but the beam does not excite plasma waves.

– the beam electrons with great longitudinal and small transverse velocities fill the loss cone, while the electrons with great transverse and small longitudinal velocities enrich the DGH function f_2 with additional electrons, then an enhanced brightness of zebra stripes is observed.

If even one of these conditions is broken, the ZP can hardly appear. The authors conclude that the described scheme quite naturally explains the (at first glance enigmatic) appearance of a zebra pattern during the electron beam passage without a type III burst in emission. However, two distributions (DGH and loss-cone) can exist simultaneously but in rather different places of the radio source.

We should also observe several properties of ZP stripes in the spectrum that were not noted in Zlotnik et al. (2009). Not all the type III-like envelopes have negative frequency drift; it is possible to note almost instantaneous changes in the broadband (07:06:31 UT) or even cases showing positive drift (07:06:25 UT). A ZP is visible between the envelopes. It is possible to trace continuous ZP stripes lasting through five envelopes with the spasmodically changing drift. The ZP is only strengthened during the envelopes and it experienced the sharp jumps in drift (by zigzags).

Such almost vertical pulsating envelopes of the ZP are not rare phenomena. For instance, let us see an excellent sample in figure 6(c) in Slottje (1972). In the event from 1974 July 3, similar ZP envelopes were continuing during several hours (Slottje 1981; Chernov 1976b). Smooth or abrupt changes in the frequency drift of ZP stripes in the event on 1994 October 25 were discussed in Chernov (2005) on the basis of the natural mechanism of the formation of stripes in absorption due to the diffusion of fast particles in whistlers. The whistler waves are always generated simultaneously with the plasma waves at an upper hybrid frequency by fast particles with a loss-cone velocity distribution. This diffusion process is examined in Chernov (1990) and in more detail in Chernov (1996, 2005). The important feature was noted there: the changes in the sign of the frequency drift correlate with the change in the direction of the spatial drift of the ZP radio source (see figs. 32

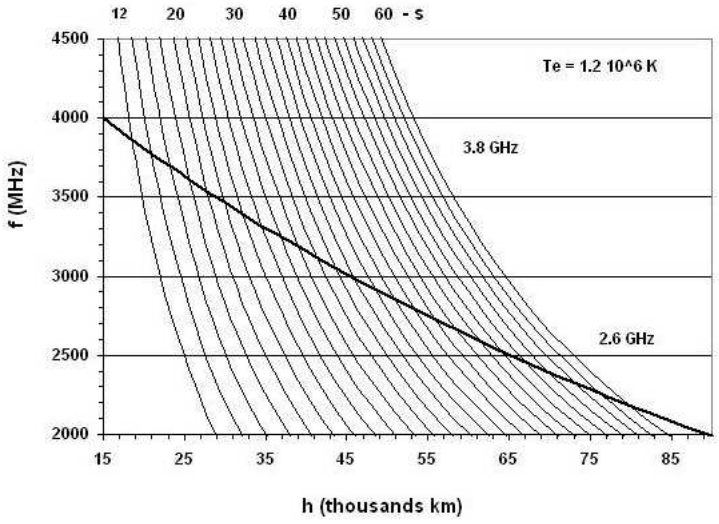

Fig. 21 Altitude dependence of the plasma frequency in accordance with the barometric law (*heavy line*) and altitude profiles of the electron cyclotron harmonics s (*light lines*) in the solar corona. For the electron temperature T_e = 1.2 $\times$ 10^6 K and initial frequency $f_{P0} = 3800$ MHz at an altitude of $h_{B0} = 20\,000$ km, 34 DPR levels form between 2600 to 3800 MHz in the plasma layers (from Laptuhov & Chernov 2010).

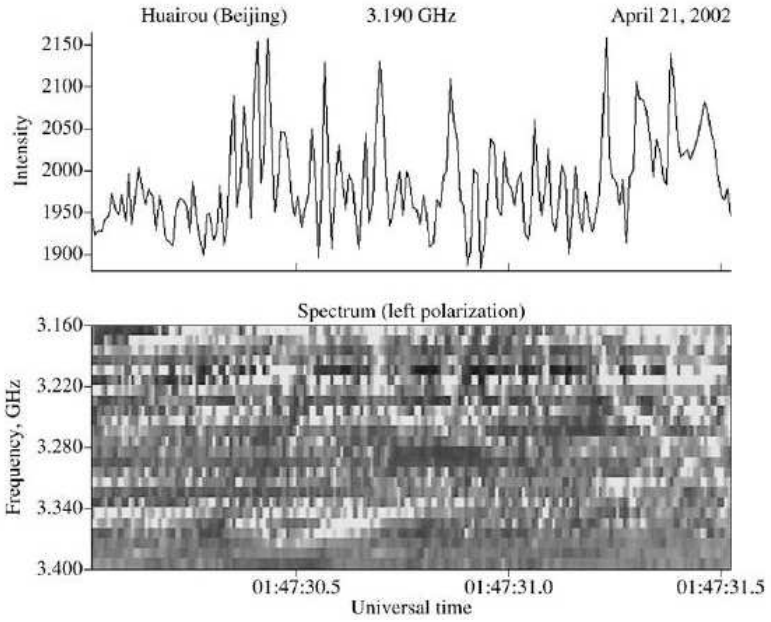

Fig. 22 Superfine structure of the continuum in the form of spikes with a period of ∼30 ms (from Laptuhov & Chernov 2010).

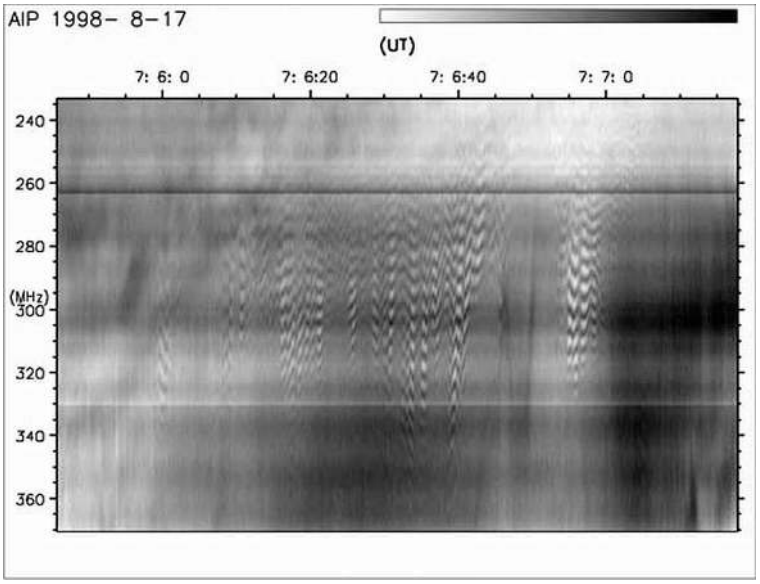

Fig. 23 Dynamic radio spectrum with zebra patterns in fast drifting envelopes recorded on 1998 August 17 by the spectrograph of the Astrophysical Institute Potsdam (from Zlotnik et al. 2009).

and 64 in Chernov 2006). The loss-cone distribution function changes due to the diffusion and the whistler generation switches from normal Doppler resonance to an anomalous one. In such a case, the whistler group velocity changes its direction to the opposite, which results in the change of sign of the frequency drift of ZP stripes. Additional particle injection can only accelerate this process and strengthen the instability of whistlers, which can be related to the strengthening of the ZP in drifting envelopes in the event examined in Zlotnik et al. (2009).

Thus, in the model with the whistlers, the absorptive ZP stripes are not formed due to the quenching of the loss-cone instability, but due to only the scattering of fast particles on whistlers and only in the whistler wave packet volume. This mechanism explains the spasmodically changing frequency drift, and it does not require any strict specific complementary parameters.

The appearance of absorptive bursts depends strongly on parameters of new beams. Chen & Yan (2008) showed that the large scale beams with longtime injection ($\sim$ 1 s) are responsible for broadband type III-like absorptive bursts, and only the small scale beams with very short injection times ($\sim$0.2 ms) could be responsible for absorptive spikes (see fig. 7 in Chen & Yan 2008). New beams with great longitudinal velocities enrich the whistler generation in anomalous Doppler resonance (Chernov 1996) and, as a consequence, the formation of ZP stripes. This explains the strengthening of ZP stripes observed during drifting envelopes (Fig. 23). We could propose that the same effect is included in bright ZP stripes in absorptive type III-like bursts in the event on 2006 December 13 (Fig. 12). However, in such a case, the whistler generation and, as a consequence, the formation of ZP stripes also depend strongly on the velocity distribution in the new beams.

In the recent small critical review of Zlotnik (2009), the advantages of the DPR model and the main failures of the model with whistlers are refined. The author asserts that the theory based on the DPR effect is the best-developed theory for ZP origin at meter-decimeter wavelengths at the present time. It explains in a natural way the fundamental ZP feature, namely, the harmonic structure (frequency spacing, numerous stripes, frequency drift, etc.) and gives a good fit for the observed radio spectrum peculiarities with quite reasonable parameters of the radiating electrons and coronal plasma. The statement that the theory based on whistlers is able to explain only a single stripe (e.g., a fiber burst) was made in Zlotnik (2009) without the correct ideas of whistler excitation and propagation in the solar corona.

First of all, Zlotnik uses the wrong term "oscillation period" of whistlers. Actually, the loss-cone particle distribution is formed as a result of several passages of the particles in the magnetic trap. However, the whistler amplification length is always small (on the order of $\leq 10^8$ cm in comparison with the length of the magnetic trap being $> 10^9$ cm) for any energy of fast particles (Breizmann 1987; Stepanov & Tsap 1999). According to Gladd (1983), the growth rate of whistlers for relativistic energies of fast particles decreases slightly if the full relativistic dispersion is used. In this case, the whistlers are excited by anisotropic electron distributions due to anomalous Doppler cyclotron resonance. Thus, our conclusion that the entire magnetic trap can be divided into intermittent layers of whistler amplification and absorption, remains valid for a broad energy range of fast particles.

In Zlotnik (2009), the main matter which is ignored is that the model involves quasilinear interactions of whistlers with fast particles, allowing one to explain all the fine effects of the ZP dynamics, mainly the superfine structure of ZP stripes and the oscillating frequency drift of the stripes which occurs synchronously with the spatial drift of radio sources.

4.2 Models of ZP Formation during Radio Wave Propagation in the Corona

Let us consider the capabilities of alternative models. One of the first such models was proposed in Laptuhov et al. (2005) and further developed in Laptuhov & Chernov (2006), where a one-dimensional inhomogeneity was considered in which the plasma and field parameters varied periodically in space along one coordinate x with a period $L_x = L$ (e.g., in the presence of nonlinear

thermal structures) and the magnetic field $\boldsymbol{B}$ = (0, 0, B) was perpendicular to the inhomogeneity gradient and directed along the z axis.

The wave equation obtained from Maxwell's equations and hydrodynamic equations for the perturbed velocity of electrons and ions in a cold nonuniform magnetoactive plasma yields a generalized vector equation for the perturbed electric field, which has separate solutions for ordinary and extraordinary waves. The problem is reduced to deriving the corresponding dispersion relations in a spatially inhomogeneous medium in which the profiles of both the plasma density and magnetic field are approximated by stepwise functions. An analysis of the solutions to this problem revealed the existence of transparent regions separated by opaque regions of different widths depending on the inhomogeneity scale L.

Thus, the dark ZP stripes observed in the radio emission spectrum can form due to the existence of opaque regions in a spatially periodic medium. The frequency separation between transparent regions increases with frequency (in agreement with observations). The number of harmonics grows with increasing amplitude of the inhomogeneity, but is independent of the ratio of the plasma frequency to the gyrofrequency in the source. This may help to overcome all the difficulties in explaining the large number of ZP stripes and small values of the magnetic field determined from the frequency separation of stripes (e.g., in the DPR-based model).

At practically the same time, Bárta & Karlický (2006) analyzed a similar problem in which the formation of harmonics during the propagation of a wave through regular inhomogeneities (such as oscillations behind a shock front) was considered in a simplified approach. The wave equation was written for an unmagnetized plasma, the dispersion relations for harmonics were not derived, and solutions for the amplitudes of reflected and transmitted waves were searched. From the conservation laws and boundary conditions admitting the existence of nontrivial solutions, the frequency dependence of the transmission coefficient was found. As a result, multiple narrow harmonics (transmission regions, called interference stripes) separated by opacity (reflection) regions were obtained. In view of analogy with the results of Laptuhov & Chernnov (2006), it is worth comparing the parameters of transmission regions obtained in these two papers.

In Ledenev et al. (2006), a similar problem was considered in an even simpler approach in which the interference pattern produced by the incident rays and those reflected from regular inhomogeneities was analyzed. The problem was solved in the geometrical optics approximation by using the eikonal equation (by analogy with the problem of light propagation through a crystal lattice). The size of the radio emission source was assumed to be infinitely small, and the emission spectrum was considered to be sufficiently broad. Evidently, in case of radio wave reflection from smooth inhomogeneities, the interference pattern cannot show as much contrast as that produced by light reflected from a solid body. Moreover, the ordinary and extraordinary waves are reflected from layers with different plasma densities. Therefore, the modulation depth of the total interference pattern produced by many small-sized sources is relatively small.

In Laptuhov & Chernov (2006), the propagation of electromagnetic waves through a spatially periodic plasma was investigated to explain the ZPs observed in solar radio bursts. The possibility of existence of one-dimensional spatially periodic structures in the solar atmosphere was demonstrated in Kovalev (1990); Laptuhov (1991) and Laptuhov & Chernov (2006) assumed that the waves propagate in an unbounded collisionless plasma along the x axis perpendicular to the magnetic field $\boldsymbol{B} = (0, 0, B(x))$.

In Laptuhov & Chernov (2009), a more realistic model in which a spatially periodic plasma occupies a region of thickness NL containing N identical plasma layers of thickness L was considered. For simplicity, each layer is assumed to consist of two piecewise-homogeneous layers with thicknesses $a < L$ and $b = L - a$. In the regions $x < 0$ and $x > NL$, the plasma is uniform.

Let us consider the propagation of broadband radio emission in such a plasma. As a matter of fact, the region occupied by the spatially periodic plasma is a frequency filter with multiple trans-

parency windows separated by opaque regions (see fig. 1 in Laptuhov & Chernov 2006). If broadband radiation is incident on the filter input ($x = 0$), then, at the output ($x = NL$), the radiation spectrum will only contain the frequencies that correspond to the transparency windows of the filter, while the amplitudes of waves with frequencies corresponding to opaque regions will be practically zero. As a result, after passing through such a filter, a structure similar to the ZP observed in the solar radio spectrum will form. This is the essence of the physical mechanism that was proposed in Laptuhov & Chernov (2006) to explain the ZP formation in solar radio emission. In this case, the mechanism for the generation of primary broadband radio emission can be arbitrary (e.g., beam – plasma or cyclotron loss-cone instability (Zheleznyakov 1995).

Let us first analyze the propagation of an ordinary wave, the field of which is described by the following simple formula (see eq. (8) in Laptuhov & Chernov 2006):

$$\frac{d^2E}{dx^2} + k^2E = 0, \;\; k^2 = \frac{\omega^2 - \omega_p^2}{c^2}, \;\; \omega_p^2 \equiv \omega_e^2 + \omega_i^2. \tag{7}$$

The plasma frequency $\omega_{\rm p}(x)$ and the corresponding constants k_m in different plasma regions are defined by the formulas

$$\begin{array}{l} \omega_{\rm p}(-\infty < x < 0) = \omega_0, \;\; \omega_{\rm p}(NL < x < \infty) = \omega_3, \\ \omega_{\rm p}[(n-1)L < x < a + (n-1)L] = \omega_1, \;\; n = 1, 2...N, \\ \omega_{\rm p}[a + (n-1)L < x < nL] = \omega_2, \;\; \omega_0 \geqslant \omega_3 \geqslant \omega_1, \\ k_m \equiv \sqrt{(\omega^2 - \omega_m^2)}/c, \;\; m = 0, 1, 2, 3, \end{array} \tag{8}$$

where all of the four frequencies ω_j ($j = 0, 1, 2, 3$) are constant. In this case, it is assumed that in the regions $x < 0$ and $x > NL$ the plasma is uniform, and between them ($0 < x < NL$) is located N of the identical layers, each of which is piecewise-uniform and has thickness L. Let an electromagnetic wave with frequency $\omega > \omega_0$ propagate along the x axis in the region $x < 0$. Then, taking into account wave reflection from the region $0 < x < NL$, a general solution to Equation (7) in the region $x < 0$ can be written as

$$E(x < 0) = E_0 \exp(ik_0 x) + E_{\rm r} \exp(-ik_0 x), \tag{9}$$

where E_0 is the amplitude of the incident wave, which is assumed to be given, and $E_{\rm r}$ is the amplitude of the reflected wave.

In the region $x > NL$, there is only the transmitted wave. Therefore, in this region, we have

$$E(x \geqslant NL) = E_{\rm t} \exp[ik_3(x - NL)]. \tag{10}$$

After simple manipulations, we obtain the transmission and reflection coefficients

$$K_{\rm t} \equiv \mathrm{mod}\left(\frac{k_3 E_{\rm t}^2}{k_0 E_0^2}\right), K_{\rm r} = \mathrm{mod}\left(\frac{E_{\rm r}^2}{E_0^2}\right) = 1 - K_{\rm t}\,. \tag{11}$$

By definition, the coefficient $K_{\rm t}$ is equal to the ratio of the intensity $\boldsymbol{Q} = c\,[\boldsymbol{E}, \boldsymbol{B}]/4\pi$ of the transmitted wave to that of the incident wave. It can easily be shown that the coefficient of reflection from N inhomogeneous plasma layers is $K_{\rm r} = 1 - K_{\rm t}$.

Note that the results obtained can also be generalized to the case of extraordinary waves described by equation (17) in Laptuhov & Chernov (2006) (cf. Eq. (7)). Below, we will consider some examples of calculating the reflection and transmission coefficients for different parameters of plasma inhomogeneities.

The number of stripes and their shape depend on the parameters (such as the size and number) of inhomogeneities. The profile of the harmonics of the reflection coefficient in the form of narrow peaks separated by relatively wide frequency intervals (see Fig. 24) can be interpreted as radiation

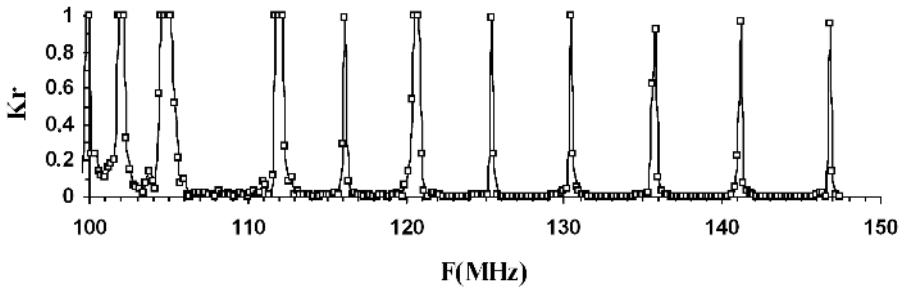

Fig. 24 Reflection coefficient $K_{\rm r}$ of ordinary waves as a function of the frequency F for $n_1 = n_2 \cdot 0.84 = n_3$, $n_0 = n_2$, $a = b = 10\,\mathrm{m}$, $n_2 = 1.2d + 8$, and $N = 50$ (from Laptuhov & Chernov 2009).

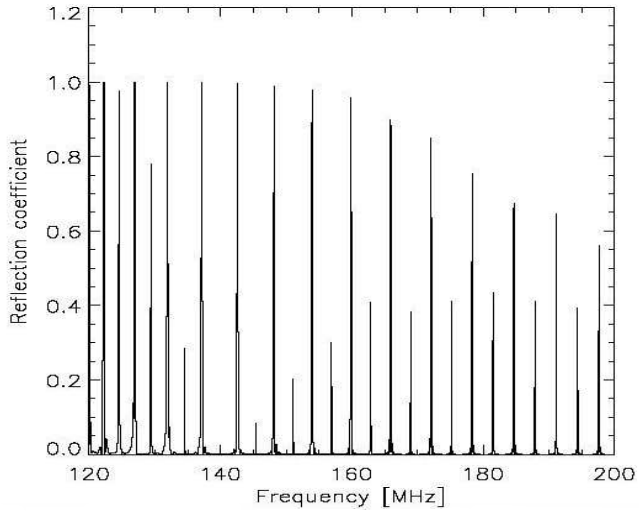

Fig. 25 Reflection coefficient $R = 1 - T$ for the series of 50 density wells produced by the density drop as a function of the frequency of an incident wave (from Bárta & Karlický 2006).

stripes similar to those present in the lower spectrum in figure 16 in Chernov (2006). Thus, in this case, the ZP is probably observed in reflected radiation. Note that the harmonics of the reflection coefficient in Figure 24 agree better with observations than the results of similar calculations in Bárta & Karlický (2006) presented in Figure 25. In our case, this is an even comb of harmonics in which the frequency separation between neighboring harmonics increases gradually with frequency, whereas in Bárta & Karlický (2006), intense harmonics alternate with weak ones. Presumably, inhomogeneities in the form of density dips, which were considered in Bárta & Karlický (2006), cannot provide the observed widths of the ZP stripes. Moreover, we take into account the fact that the magnetic field and harmonics of an ordinary wave agree better with observations.

For a smaller number of larger inhomogeneities with $a = 45\,\mathrm{m}$, the frequency profile of the transmission coefficient (see Fig. 26) yields nearly symmetric harmonics, which are most frequently observed (see the upper spectrum in fig. 16 in Chernov 2006).

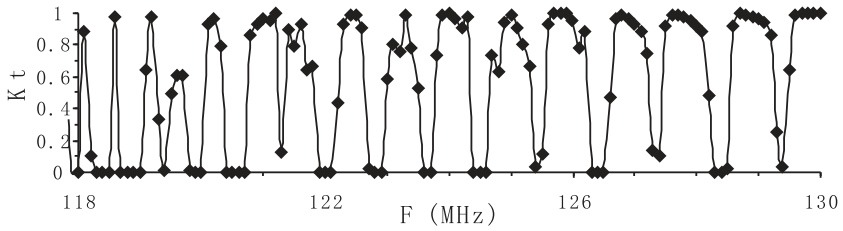

Fig. 26 Transmission coefficient $K_{\rm t}$ of ordinary waves as a function of the frequency F for $n_0 = n_3 = 1d + 8$, $n_2 = 1.5n_0$, $n_1 = n_2/2$, $a = 45\,$m, $b = a$, $N = 10$, and $B = 5\,$G (from Laptuhov & Chernov 2009).

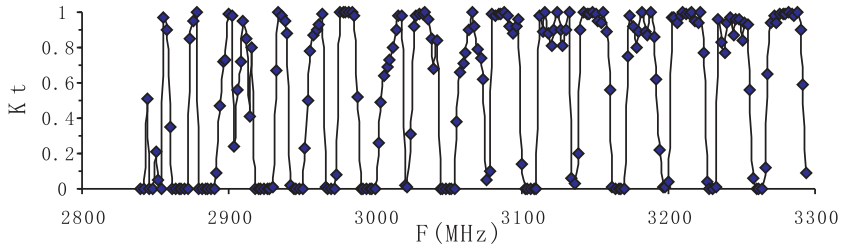

Fig. 27 Transmission coefficient $K_{\rm t}$ of ordinary waves as a function of the frequency F for $n_1 = n_2/\alpha$, $n_0 = 2n_2/(1+\alpha) = n_3$, $b = L/(1+\alpha)$, $a = \alpha b$, $L = 3\,$m, $\alpha = 2$, $n_2 = 1.0d + 11$, and $B = 100\,$G (from Laptuhov & Chernov 2009).

Figure 27 shows the results of calculations of the transmission coefficient in the microwave range. It is seen that, after passing through inhomogeneities with a thickness of $L = 3\,$m, the spectrum of ordinary waves consists of symmetric harmonics, the frequency separation between which increases gradually with frequency, which agrees with observations. A sufficiently large number of harmonics are produced when the number of inhomogeneities is > 10.

4.2.1 Some concluding remarks

An analysis of the difficulties arising in different models shows that the improvement of these models necessitates imposing new stringent conditions on the parameters of plasma and waves in the source. The simplest model is related to the propagation of radio waves through regular inhomogeneities, because inhomogeneities are always present in the solar corona. However, for the cm range the effectiveness of this model requires inhomogeneities over the size of several meters. Such scales can be produced by ion-acoustic waves or the oscillator structure of the density and the magnetic fields behind the shock wave front. Existence of such waves in the flare region with the magnetic reconnection is completely probable. The alternative mechanism of the formation of small-scale heterogeneities could be the tearing-mode instability of the current-carrying loops in the process of magnetic reconnection (Tan 2010). In this case, the dynamics of ZP stripes (variations in the

frequency drift, stripe breaks, etc.) may be associated with the propagation of inhomogeneities, their evolution, and their disappearance.

The observed frequency difference between neighboring ZP stripes increases with frequency. This corresponds to the propagation of ordinary waves, the electric field of which is parallel to the unperturbed magnetic field, through a spatially periodic plasma. The number of discrete harmonics does not depend on the ratio of the plasma frequency to the gyrofrequency in the source. The latter circumstance can eliminate all the difficulties that arise in explaining the large number of ZP stripes and the small magnetic field value determined from the frequency separation of stripes (e.g., in the DPR based model).

The superfine structure observed in the microwave range, when all the continuous emission consists of spikes (Fig. 20), indicates the presence of plasma wave – whistler interaction in the pulsed regime of whistler interaction with ion acoustic waves in the radio emission source generating ordinary waves (this mechanism was considered in Chernov et al. (2003)). An alternative source of pulsed radio emission may be associated with plasma density pulsations caused by the propagation of a finite amplitude wave. The generation of electron cyclotron maser radiation, which is considered to be a possible cause of the observed spikes in Fleishmann & Mel'nikov (1998), is dominated by extraordinary waves.

4.3 Other Recent Models

4.3.1 Nonlinear periodic space – charged waves in plasma

Kovalev (2009) has investigated periodic nonlinear waves that can arise in plasma due to the excitation of potential oscillations by accelerated electrons with unstable distributions. As was noted in Kovalev & Petviashvili (1994), one-dimensional single-peak distributions of accelerated electrons are most likely to exist in the solar flare plasma. Such electron distributions excite resonant Langmuir oscillations with frequencies $\omega_2 <$min $\{\omega_B, \omega_P\}$, due to the anomalous Doppler resonance. Low- and high-frequency modes of Langmuir oscillations can form large-amplitude periodic nonlinear waves. The corresponding spectrum of electromagnetic waves excited resonantly by the current of a potential wave is calculated. It is shown that an equidistant spectrum of electromagnetic radiation in plasma can form in the presence of a periodic potential wave.

Thus, the radio emission harmonics can be generated directly in the source in the form of a nonlinear periodic space charge wave in plasma. In Kovalev (2009), a solution in the form of such a wave propagating in a magnetic field was obtained using the hydrodynamic approach (without taking into account wave dispersion). The spectrum near the breaking point, in the vicinity of which the number of harmonics increases substantially, was calculated. Due to electron bunching, the periodic wave with the spatial period $l = 2\pi u/\omega_2$ has the form of spatially alternating negatively and positively charged layers with an increased and a decreased electron density. In the presence of a wave electric field, the accelerated particles are subject to additional periodic acceleration and deceleration, due to which an electromagnetic wave is generated.

For a sufficiently large amplitude of density oscillations (a), a large number of harmonics with frequency separation close to the electron-cyclotron frequency can be excited. The number of these harmonics is determined by the parameter $N = \frac{3}{2^{3/2}(1-a)^{3/2}}$, which characterizes the degree of nonlinearity. Thus, for $a \sim 0.9$, we have $N \approx 34$. Since the radio emission can be generated in a relatively small-size source, the key difficulty of the DPR-based model, namely, the excitation of a large number of harmonics in a distributed source, is overcome (Fig. 20). The number of harmonics can be fairly large when one of the plasma oscillation modes is dominant. In this case, the amplitudes of harmonics decrease fairly slowly ($\propto s^{-1/3}$) with increasing harmonic number s.

Due to inverse processes, the energy of background electromagnetic waves can transform into the energy of potential oscillations at the resonance frequencies $s\omega_2$. This can lead to the formation of an absorption zebra pattern consisting of stripes with a depressed radiation intensity.

The efficiency of the quite natural mechanism associated with nonlinear space charge waves depends on whether strong nonlinearity is reached; however, conditions for achieving the nonlinear regime were not considered in Kovalev (2009). The nonlinearity should rapidly increase and disappear in the course of wavebreaking (at a = 1).

4.3.2 The new alternative mechanism of the ZP due to development of explosive instability in the system beam – plasma

Observations of ZPs during powerful flares make it possible to assume that the particle acceleration to relativistic velocities and excitation of different wave modes occur in the radio source. Therefore, probably, other possible interactions of waves and particles should be taken into account. For example, in Fomichev & Fainshtein (1981) was proposed the decay instability of whistlers to the harmonics of the ion sound, which have weak spatial dispersion and small damping at frequencies much less than the ion Langmuir frequency $\omega_{\rm oi}$. In Fomichev et al. (2009) an alternative mechanism of ZPs is discussed, due to the development of explosive instability in the system, which is a weakly relativistic beam with nonisothermic plasma. The explosive instability appears in the nonequilibrium system, where there are waves of negative energy (Kadomtsev et al. 1964), moreover, in the resonance triplet the wave of the highest frequency of ω_3 must possess negative energy, and the two lowest waves ($\omega_{1,2}$) have positive energy. Fomichev et al. (2009) have shown that the mechanism of the generation of the ion-acoustic "saw" as a result of the development of explosive instability in the system with a weakly relativistic flow of protons and strongly nonisothermic plasma is more effective in the energy sense.

The number of harmonics of ionic sound n is determined by two factors: 1) the dispersion of ion sound must be sufficiently small [1]; 2) $\nu_{\rm ef} \ll \omega$ (ω – the angular frequency of sound), i.e., the n-harmonic of sound must weakly attenuate.

The quasi-hydrodynamic approximation was utilized for describing the interaction of the particles of the beam and plasma (Fainshtein & Chernova 1996; Ginzburg 1967). Linearizing the hydrodynamic equations for the processes of $\sim \exp(i\omega t - ikx)$, a dispersion equation for the system of flow–plasma was obtained:

$$1 \; - \frac{\omega_{0i}^2}{\omega} \; - \frac{\omega_{0i}^2}{c_s^2 k^2} \; - \; \frac{\omega_{0s}^2}{(\omega \; - \; kV_0)^2 \; \left(1 \; - \; \frac{\omega - ck}{3ck}\right)} \; = \; 0, \tag{12}$$

where $\omega_{0s}^2 \; = \; 4\,\pi e^2\, N_{0s}\, M_0^{-1}, \omega_{0i}^2 \; = \; 4\,\pi e^2\, N_0\, M^{-1}$, ω is the cyclic frequency, k is the wave number; e, M_o, M – electron charge, the rest mass of the ion beam, and the mass of the ion of the plasma respectively; $\bar{\rho}_s \; = \; N_{0s} \; + \; \rho_s\,; \bar{V}_s \; = \; V_0 \; + \; V_s\,; \rho_s\,,\; V_s\,,\; \rho_i\,,\; V_i$ – the deviation respectively of ion concentrations of the beam, speed of the ions of beam, concentration of the ions of plasma, and velocity of the ions of plasma from their equilibrium values $N_{0s},\; V_0, N_0, 0$. With $V_0/c_s \; \gg \; 1,\; N_{0s}/N_0 \; \ll \; 1$ from (12) the approximate dispersion equations were obtained:

$$\omega_1 \; \equiv \; \Omega \; \approx \; \; c_s\, k_1 \; \equiv \; c_s m\, q\,; \tag{13}$$

$$\omega_{3,2} \; - k_{3,2}\, V_0 \; \approx \; \mp\, \omega_{0s} \; + \; \delta\,; \qquad \frac{\delta}{\omega_{0s}} \ll 1\,. \tag{14}$$

[1] $n^2 q^2 c_s^2 \omega_{\rm oi}^2$; q – wave number of the base ion-sound mode; c_s – ion-sound speed ($c_s^2 = \alpha T_{\rm e} M^{-1}$), M – ion mass, α– Boltzmann constant.

Equation (13) describes the ion-acoustic wave (energy positive), and (14) slow (ω_3, negative energy) and rapid (ω_2, positive energy) beam waves. The number $m > 0$ is selected from the escape condition of radio emission from the corona. It is easy to determine that for the slow beam wave (ω_3, k_3), the fast beam wave (ω_2, k_2) and the sound (Ω, q) the conditions of synchronism are satisfied (Tsytovich 1970). From taking the conditions of synchronism into account (13), (14) we will obtain:

$$mq \approx 2\,\omega_{0s}\,V_0^{-1}\,. \tag{15}$$

Since the sound has weak dispersion, the cascade process is possible:

$$mq + mq \rightarrow 2mq + mq \rightarrow 3mq + mq \ldots mnq.$$

Then, after decomposing nonlinear terms in (1) up to the quadratic terms and after using the standard procedure in the weak turbulence (Weiland & Wilhelmsson 1977; Tsytovich 1970), the shortened equations for the complex amplitudes of coupling modes are obtained: beam modes $a_j(j = 1, 2)$ and ion sound $b_k(k = 1, 2, \ldots mn)$. The analysis of interaction coefficients showed that the systems of such equations describe the stabilized "explosion" (Fainshtein 1976).

It is also shown that the increment of the growth of ion sound in this case considerably exceeds the values obtained in Fomichev & Fainshtein (1981). Therefore, the mechanism in question occurs much more effectively.

The generable sound is scattered over the fast protons, which move with a speed of $V \sim V_0 \sim 10^{10}$ cm s^{-1} and, according to the mechanism described in Fomichev & Faishtein (1981), the radiation from the source frequency is $\omega^t \approx mqnV$, and frequency separation between the stripes is $\delta\omega^t = mqV$. Taking into account Equation (15) and selected parameters ($N_0 \sim 5 \times 10^9$ cm^{-3}, $N_s \cdot N_0^{-1} \sim 10^{-3}$, the constant magnetic field ~ 30 G) we obtain, for the emission frequency of $\geqslant 634$ MHz, the value of coefficient $m = 15$, ($7 \times 10^2 \leqslant mn \ll 15 \times 10^3$) and the frequency separation between the adjacent stripes $\delta\omega^t \approx 15$ MHz. The obtained value of $\delta\omega^t$ corresponds to the observed frequency separation in the decimeter wave band (Chernov 2006). In the above given estimations, the wavelength of the ion sound ~ 100 m, the initial frequency $\sim$1.0 kHz and the cyclic frequency of the slow beam wave $\omega_3 \sim 7 \times 10^2\ \omega_{0i}$ (that correspond to ~ 10 GHz).

Discrete emission bands are possible when the width of each emission band will be less than the value of the frequency separation. This condition imposes a restriction on the dispersion of the beam velocities. As shown in such estimations, and implemented in Fomichev & Fainshtein (1981), the beam of protons must be sufficiently quasi-monoenergetic in the case in question, $\Delta V_0/V_0 < 10^{-3}$.

5 CONCLUSIONS

We have considered several of the most recent events with new peculiar elements of zebra patterns. All new properties are considered in light of both what was known earlier and new theoretical models.

In two events (2004 July 24 and 2004 November 3), the large-scale ZP consisted of small-scale fiber bursts. The appearance of such an uncommon fine structure is connected with the following special features of the plasma wave excitation in the radio source: both whistler and plasma wave instabilities are too weak at the very beginning of the events (the continuum was absent), and the fine structure is almost invisible. Then, whistlers generated directly at DPR levels "highlight" the radio emission only from these levels due to their interaction with plasma waves.

A unique fine structure was observed in the event on 2006 December 13: spikes in absorption formed darks ZP stripes against the absorptive type III-like bursts. The spikes in absorption can appear in accordance with the well known mechanism of absorptive bursts. The additional injection of fast particles filled the loss-cone (breaking the loss-cone distribution), and the generation of the

continuum was quenched at these moments, which was evidenced by the formation of bursts in absorption. The maximum absorptive effect occurred at the DPR levels. The parameters of millisecond spikes are determined by small dimensions of the particle beams and local scale heights in the radio source.

Thus, in each new event, the new special features of the fine structure are revealed. However, they are usually related with the varied conditions in the source. In such a case, one ought not to find the special emission mechanism for each event, which was repeatedly done before.

The DPR model helped to understand several aspects of unusual elements of ZPs. In this connection, the calculations of growth rates of upper hybrid waves with a different distribution function of fast electrons inside of the loss-cone is very important (Kuzneysov & Tsap 2007). However, discussions concerning the validity of taking into account one or several harmonics in a hybrid band continue. At the same time, Laptuhov & Chernov (2009) showed that the simultaneous existence of several tens of the DPD levels in the corona is impossible for any realistic profile of the plasma density and magnetic field (if we do not assume the order of magnitude of the local density and magnetic field scale heights to be smaller).

Since all known models still have deficiencies, the attempts to create new theories continue. We examined three new theories.

The formation of transparency and opacity bands during the propagation of radio waves through regular coronal inhomogeneities is the most natural and promising mechanism. It explains all main parameters of a regular ZP. The dynamics of ZP stripes (variations in the frequency drift, stripe breaks, etc.) can be associated with the propagation of inhomogeneities, their evolution, and disappearance. Inhomogeneities are always present in the solar corona, however direct evidence of the existence of inhomogeneities with the scales of several meters in the corona are absent, although ion-sound waves could serve this purpose.

The model of a nonlinear periodic space, charged waves in plasma (Kovalev 2009), is also a very natural mechanism in the solar flare plasma. However, in the case of intrinsic plasma emission, it gives a constant frequency separation between stripes of $\approx \omega_B$, while the observations verify the increase of the frequency separation with frequency. In addition, the condition of achieving strong nonlinearity remains uncertain.

The mechanism of scattering fast protons in ion-sound harmonics in explosive instability looks very uncommon, and it requires a number of strict conditions. Although the fast protons always exist in large flares, the presence of nonisothermic plasma is completely feasible in the shock wave fronts.

The last two models could be useful in describing large radio bursts. All three models are related to a compact radio source. The number of discrete harmonics does not depend on the ratio of the plasma frequency to the gyrofrequency in the development of all three models. The latter circumstance can eliminate all the difficulties that arise in the DPR model.

Acknowledgements We are grateful to the Nobeyama, TRACE, RHESSI and SOHO (LASCO/EIT) teams for operating the instruments and performing the basic data reduction, and especially for their open data policies. G.P. Chernov appreciates the support of the Chinese Academy of Sciences and NSF of China, with Prof. Yan Yihua, which enabled this work with NAOC colleagues, as well as the Russian Foundation of Basic Research (RFBR), grant Nos. 08–02–00270 and 11–02–91151.

References

Abada-Simon, M., Lecacheux, A., Louran, P., Dulk, G. A., Belkora, L., Bookbinder, J. A., & Rosolen, C. 1995, in IAU Coll. 151, Flares and Flashes, Monograph, eds. J. Grenier et al., 454, 32
Aschwanden, M. J. 2004, Physics of the Solar Corona (Pruxis Publishing)
Bárta, M., & Karlický, M. 2001, A&A, 379, 1045
Bárta, M., & Karlický, M. 2006, A&A, 450, 359
Benz, A. O., & Kuijpers, J. 1976, Sol. Phys., 46, 275
Breizman, B. N. 1987, in Problems in Plasma Theory, ed. B. B. Kadomtsev (Moscow: Energoizdat), 15, 55
Chen, B., & Yan, Y. 2008, ApJ, 689, 1412
Chernov, G. P. 1976a, Soviet Astronomy, 20, 582
Chernov, G. P. 1976b, Soviet Astronomy, 20, 449
Chernov, G. P. 1990, Sol. Phys., 130, 75
Chernov, G. P. 1996, Astronomy Reports, 40, 561
Chernov, G. P. 1997, Astronomy Letters, 23, 827
Chernov, G. P. 2005, Plasma Physics Reports, 31, 314
Chernov, G. P. 2006, Space Science Reviews, 127, 195
Chernov, G. P., Markeev, A. K., Poquerusse, M., et al. 1998, A&A, 334, 314
Chernov, G. P., Yasnov, L. V., Yan, Y.-H., & Fu, Q.-J. 2001, ChJAA (Chin. J. Astron. Astrophys.), 1, 525
Chernov, G. P., Yan, Y. H., & Fu, Q. J. 2003, A&A, 406, 1071
Chernov, G. P., Yan, Y. H., Fu, Q. J., & Tan, C. M. 2005, A&A, 437, 1047
Chernov, G. P., Yan, Y., Fu, Q., Tan, C., & Wang, S. 2008, Sol. Phys., 250, 115
Chernov, G. P., Yan, Y. H., Tan, C. M., Chen, B., & Fu, Q. J. 2010, Sol. Phys., 262, 149
Dąbrowski, B. P., Rudawy, P., Falewicz, R., Siarkowski, M., & Kus, A. J. 2005, A&A, 434, 1139
Dory, R. A., Guest, G. E., & Harris, E. G. 1965, Phys. Rev. Lett., 14, 131
Dulk, G. A., & McLean, D. J. 1978, Sol. Phys., 57, 279
Fainshtein, S. M. 1976, Zhurnal Eksperimental noi i Teoreticheskoi Fiziki, 71, 1021 (Sov. Phys. JETP 44, 534)
Fainstein, S. M., & Chernova, E. A. 1996, Zh. Eksp. Teor. Fiz., 109, 821 (1996, JETP, 82, 442)
Fleishman, G. D., Stepanov, A. V., & Yurovsky, Y. F. 1994, Sol. Phys., 153, 403
Fleishman, G. D., & Mel'Nikov, V. F. 1998, Usp. Fiz. Nauk 168, 1265 (Soviet Physics Uspekhi, 41, 1157)
Fomichev, V. V., & Fainshtein, S. M. 1981, Sol. Phys., 71, 385
Fomichev, V. V., Fainshtein, S. M., & Chernov, G. P. 2009, Plasma Physics Reports, 35, 1032
Fu, Q., et al. 2004, Sol. Phys., 222, 167
Ginzburg, V. L. 1967, Propagation of Electromagnetic Waves in Plasma, Íoscow, Nauka
Ginzburg, V. L., & Ruchadze, A. A. 1975, Volny v magnitoaktivnoj plazme., eds. V. L. Ginzburg, & A. A. Ruchadze (Moskva: Nauka) 256 (in Russian)
Gladd, N. T. 1983, Physics of Fluids, 26, 974
Guo, Y., Ding, M. D., Wiegelmann, T., & Li, H. 2008, ApJ, 679, 1629
Huang, G.-L. 2003, New Astronomy, 8, 213
Huang, G.-L. 2004, Proceedings of the IAU Symposium 226, eds. K. Dere, J. Wang, & Y. Yan (Cambridge University Press), 95
Huang, J., Yan, Y., & Liu, Y. 2007, Advances in Space Research, 39, 1439
Kadomtsev, B. B., Mihailovsky, A. B., & Timifeev, A. V. 1964, Zh. Eksp. Teor. Fiz. 47, 2266 (Sov. Phys. JETP 20, 1517)
Karlický, M., & Bárta, M. 2007, Advances in Space Research, 39, 1415
Karlický, M., Bárta, M., Jiřička, K., et al. 2001, A&A, 375, 638
Klassen, A. 1996, Sol. Phys., 167, 449

Kovalev, V. A. 1990, Kinematika i Fizika Nebesnykh Tel, 6, 38
Kovalev, V. A. 2009, Plasma Physics Reports, 35, 394
Kovalev, V. A., & Petviashvili, V. I. 1994, Russian Phys. J., 37, 699 (Russ. Izv. Vyssh. Uchebn. Zaved., Fiz., No. 7, 118)
Krishan, V., Fernandes, F. C. R., Cecatto, J. R., & Sawant, H. S. 2003, Sol. Phys., 215, 147
Krueger, A. 1979, Geophysics and Astrophysics Monographs, Dordrecht: Reidel, 1979
Kuijpers, J. M. E. 1975a, Collective wave-particle interactions in solar type IV radio source, Ph.D Thesis (Utrecht University)
Kuijpers, J. 1975b, Sol. Phys., 44, 173
Kuznetsov, A. A. 2007, Astronomy Lett., 33, 319
Kuznetsov, A. A. 2008, Sol. Phys., 253, 103
Kuznetsov, A. A., & Tsap, Y. T. 2007, Sol. Phys., 241, 127
LaBelle, J., Treumann, R. A., Yoon, P. H., & Karlicky, M. 2003, ApJ, 593, 1195
Laptukhov, A. I. 1991, in Interplanetary Medium and Magnetospheric Processes, Nauka, Moscow (in Russian)
Laptukhov, A. I., & Chernov, G. P. 2006, Plasma Physics Reports, 32, 866
Laptukhov, A. I., & Chernov, G. P. 2009, Plasma Physics Reports, 35, 160
Laptuhov, A. I., Chernov, G. P., & Kovalev, V. A. 2005, in International Symposium, Astronomy-2005: Current State and Prospects (Moscow), Book of Abstracts, Paper P2.31; Tr. GAISh 78, 31
Ledenev, V. G., Karlický, M., Yan, Y., & Fu, Q. 2001, Sol. Phys., 202, 71
Ledenev, V. G., Yan, Y., & Fu, Q. 2006, Sol. Phys., 233, 129
Lin, J., & Forbes, T. G. 2000, J. Geophys. Res., 105, 2375
Magdalenić, J., Vršnak, B., Zlobec, P., Hillaris, A., & Messerotti, M. 2006, ApJ, 642, L77
Mészárosová, H., Karlický, M., Sawant, H. S., Fernandes, F. C. R., Cecatto, J. R., & de Andrade, M. C. 2008, A&A, 491, 555
Mollwo, L. 1983, Sol. Phys., 83, 305
Mollwo, L. 1988, Sol. Phys., 116, 323
Ning, Z., Fu, Q., & Lu, Q. 2000, A&A, 364, 853
Osten, R. A., & Bastian, T. S. 2006, ApJ, 637, 1016
Pick, M., Démoulin, P., Krucker, S., Malandraki, O., & Maia, D. 2005, ApJ, 625, 1019
Priest, E., & Forbes, T. 2000, Magnetic Reconnection, eds. E. Priest, & T. Forbes (UK: Cambridge Univ. Press), 612,
Roussev, I. I., Forbes, T. G., Gombosi, T. I., et al. 2003, ApJ, 588, L45
Sawant, H. S., et al. 2002, Advances in Space Research, 29, 349
Schwenn, R., et al. 2006, Space Science Reviews, 123, 127
Slottje, C. 1972, Sol. Phys., 25, 210
Slottje, C. 1981, Atlas of fine Structures of Dynamic Spectra of Solar Type IV-dm and Some Type II Bursts, Utrecht Observatory
Stepanov, A. V. 1974, Soviet Astronomy, 17, 781
Stepanov, A. V., & Tsap, Y. T. 1999, Astronomy Reports, 43, 838
Strong, K., Bruner, M., Tarbell, T., Title, A., & Wolfson, C. J. 1994, Space Science Reviews, 70, 119
Sych, R. A., Sawant, H. S., Karlický, M., & Mészárosová, H. 2006, Advances in Space Research, 38, 979
Tan, B. 2010, Ap&SS, 325, 251
Tan, B., Yan, Y., Tan, C., & Liu, Y. 2007, ApJ, 671, 964
Tsuneta, S. 1996, ApJ, 456, 840
Tsytovich, V. N. 1970, Nonlinear Effects in Plasma (New York: Plenum Press), 1970
Wang, S. J., Yan, Y. H., Liu, Y. Y., Fu, Q. J., Tan, B. L., & Zhang, Y. 2008, Sol. Phys., 253, 133
Weiland, J., & Wilhelmsson, H. 1977, Coherent Non-linear Interaction of Waves in Plasma (Pergamon Press)

Winglee, R. M., & Dulk, G. A. 1986, ApJ, 307, 808
Wu, D. J., Huang, J., Tang, J. F., & Yan, Y. H. 2007, ApJ, 665, L171
Yan, Y., Huang, J., Chen, B., & Sakurai, T. 2007, PASJ, 59, 815
Zaitsev, V. V., & Stepanov, A. V. 1975, A&A, 45, 135
Zheleznyakov, V. V. 1995, Radiation in Astrophysical Plasmas (engl. transl. Kluwer Academic Publisher), Dordrecht (in Russ., Izdat. Nauka, Moscow, 1977).
Zheleznyakov, V. V., & Zlotnik, E. I. 1975a, Sol. Phys., 44, 447
Zheleznyakov, V. V., & Zlotnik, E. Y. 1975b, Sol. Phys., 44, 461
Zlobec, P., & Karlický, M. 2007, Sol. Phys., 246, 419
Zlotnik, E. Y. 2009, Central European Astrophysical Bulletin, 33, 281
Zlotnik, E. Y., Zaitsev, V. V., Aurass, H., Mann, G., & Hofmann, A. 2003, A&A, 410, 1011
Zlotnik, E. Y., & Sher, E. M. 2009, Izv. VUZov Radiofizika, 52, 95 (Rus), Radiophysics and Quantum Electronics, 52, 88.
Zlotnik, E. Y., Zaitsev, V. V., Aurass, H., & Mann, G. 2009, Sol. Phys., 255, 273